Biotechnology Reports 31 (2021) e00652

Contents lists available at ScienceDirect

Biotechnology Reports

journal homepage: www.elsevier.com/locate/btre

Analysis of the phosphorylome of trichoderma reesei cultivated on sugarcane bagasse suggests post-translational regulation of the secreted glycosyl hydrolase Cel7A

Wellington Ramos Pedersoli [a], Renato Graciano de Paula [b,c], Amanda Cristina Campos Antoniêto [b], Cláudia Batista Carraro [b], Iasmin Cartaxo Taveira [b], David Batista Maués [b], Maíra Pompeu Martins [a], Liliane Fraga Costa Ribeiro [b], André Ricardo de Lima Damasio [d], Rafael Silva-Rocha [e], Antônio Rossi Filho [a], Roberto N Silva [b,*]

[a] Department of Genetics, Ribeirão Preto Medical School, University of São Paulo, Ribeirão Preto, SP, 14049-900, Brazil
[b] Department of Biochemistry and Immunology, Ribeirão Preto Medical School, University of São Paulo, Ribeirão Preto, SP, 14049-900, Brazil
[c] Department of Physiological Sciences, Health Sciences Centre, Federal University of Espirito Santo, Vitória, ES, 29047-105, Brazil
[d] Department of Biochemistry and Tissue Biology, Institute of Biology, University of Campinas (UNICAMP), Campinas, SP, 13083-970, Brazil
[e] Systems and Synthetic Biology Laboratory, Department of Cell and Molecular Biology, Ribeirão Preto Medical School, University of São Paulo, Ribeirão Preto, 14049-900, Brazil

ARTICLE INFO

Keywords:
Trichoderma reesei
Phosphorylome
Sugarcane bagasse
Cel7A
Phosphorylation

ABSTRACT

Trichoderma reesei is one of the major producers of holocellulases. It is known that in *T. reesei*, protein production patterns can change in a carbon source-dependent manner. Here, we performed a phosphorylome analysis of *T. reesei* grown in the presence of sugarcane bagasse and glucose as carbon source. In presence of sugarcane bagasse, a total of 114 phosphorylated proteins were identified. Phosphoserine and phosphothreonine corresponded to 89.6% of the phosphosites and 10.4% were related to phosphotyrosine. Among the identified proteins, 65% were singly phosphorylated, 19% were doubly phosphorylated, 12% were triply phosphorylated, and 4% displayed even higher phosphorylation. Seventy-five kinases were predicted to phosphorylate the sites identified in this work, and the most frequently predicted serine/threonine kinase was PKC1. Among phosphorylated proteins, four glycosyl hydrolases were predicted to be secreted. Interestingly, Cel7A activity, the most secreted protein, was reduced to approximately 60% after *in vitro* dephosphorylation, suggesting that phosphorylation might alter Cel7A structure, substrate affinity, and targeting of the substrate to its carbohydrate-binding domain. These results suggest a novel post-translational regulation of Cel7A.

Introduction

Fungi of the genus *Trichoderma* are mesophilic ascomycetes with a wide distribution on the planet, and are mainly found in decaying plant material [1–4]. The filamentous fungus *Trichoderma reesei* is one of the major holocellulase producers [5], albeit displaying a reduced number of cellulolytic enzymes when compared to other lignocellulosic fungi [6]. The success of *T. reesei* in biomass degradation is due to an efficient system for transporting nutrients inside the cells and to the induction/secretion of holocellulases [7]. However, the regulation of the expression of these enzymes is not fully understood. In particular, lignocellulolytic enzyme production depends on the type of carbon source available for the fungus. For instance, easily metabolized carbon sources, such as glucose, repress enzyme expression. Such repression is mainly mediated by Cre1, a transcription factor that binds to the promoter of several glycosyl hydrolase (GH) genes, blocking the action of the RNA polymerase. Interestingly, the phosphorylation of Cre1 at S241 is required for DNA binding [8]. Recently, Han et al, in order to evaluate the influence of phosphorylation on the transcription factor Cre1 in *T. reesei* and its effect on the expression of cellulolytic enzymes, mutated several residues at C terminus of Cre1 to mimic dephosphorylation and observed that there was an improvement in cellulase transcription levels and activity in the presence of glucose and inhibition of carbon catabolite repression [9].

* Corresponding author.
E-mail address: rsilva@fmrp.usp.br (R.N. Silva).

https://doi.org/10.1016/j.btre.2021.e00652
Received 24 August 2020; Received in revised form 5 May 2021; Accepted 16 June 2021
Available online 22 June 2021

Phosphorylation events are known to be involved in the regulation of various cellular processes, including metabolism, transcription, translation, protein secretion and degradation, homeostasis, and signaling, as well as cell communication, proliferation, differentiation, and survival [10]. Notably, at least one third of all proteins contain covalently bonded phosphate on serine, threonine, and tyrosine at some point in time [11].

In *T. reesei*, protein phosphorylation patterns change in a carbon source-dependent manner [12]. Indeed, Nguyen et al. identified, between sophorose and spent-grain extracts, differentially phosphorylated proteins related to processes such as carbon storage, intracellular trafficking, cytoskeleton remodeling, and regulation of cellulase gene expression, highlighting the importance of understanding the phosphorylation phenomena triggered by the sensing of a specific carbon source.

Several studies have shown that sugarcane bagasse has great potential for biofuel production and can be used in the biorefinery industry [13–15]. On this type of biomass, *T. reesei* hydrolyzes cell wall polysaccharides into dimers or monomers. However, the regulation of gene expression (especially of holocellulase-coding genes) occurring when the fungus is cultivated on this carbon source is not fully understood [16, 17]. Therefore, in order to gain a broader understanding of the phosphorylation events taking place in these growth conditions and how they affect different cellular functions, we cultured *T. reesei* in the presence of sugarcane bagasse and identified phosphorylated proteins by liquid chromatography with tandem mass spectrometry (LC-MS/MS) after phosphopeptide enrichment by immobilized metal ion affinity chromatography (IMAC).

Materials and methods

Strains and cultivation conditions

The *T. reesei* QM9414 strain (ATCC 26921) was obtained from the collection of the Research Group for Synthetic Biology and Molecular Biotechnology, Institute of Chemical, Environmental, and Bioscience Engineering, Faculty of Technical Chemistry, Vienna University of Technology, Austria, and maintained in MEX medium (3% (w/v) malt extract and 2% (w/v) agar-agar) at 4°C. Initially, the fungi were grown on MEX medium at 28°C for a period of seven to 10 days until complete sporulation. For all experiments, a spore suspension of QM9414 containing 10^6 cells mL^{-1} was precultured into 200 mL of Mandels-Andreotti medium [18] supplemented with 1% (w/v) glycerol for 24 h and then transferred to 200 mL of fresh Mandels-Andreotti medium containing 1% (w/v) of sugarcane bagasse (SBC) or 2% (w/v) glucose as a control [19,20]. The cultures were incubated in an orbital shaker (180 rpm) at 28°C for 24, 48, 72, and 96 h for SBC and 24h for glucose as previously described [21] . After incubation, the mycelia were collected by filtration, frozen, and stored at -80°C. Sugarcane bagasse was kindly donated by Nardini Agroindustrial Ltd., Vista Alegre do Alto, São Paulo, Brazil, and prepared as previously described [22]. *In natura* sugarcane bagasse was briefly treated with 14 kg cm^{-2} water steam, washed exhaustively with distilled water until reducing sugars were not detected by 3,5-dinitrosalicylic acid (DNS) [23], and dried at 40 °C.

Sample preparation

For protein isolation, the obtained frozen mycelia from sugarcane bagasse and glucose cultures were ground to a fine powder using a mortar and pestle cooled in liquid nitrogen. Proteins were then extracted from the powdered samples (100 mg) using an extraction solution at pH 7.4 (0.8% NaCl, 0.02% KCl, 0.27% $Na_2HPO_4{\cdot}7H_2O$, 0.024% KH_2PO_4, 10 mM NaF, 1 mM Na_3VO_4, 0.2% phosphatase inhibitor cocktail 3 (Sigma-Aldrich, St. Louis, MO, USA, cat. n. P0044), and 0.2% protease inhibitor cocktail (protease inhibitor mix 80-6501-23, GE Healthcare, Chicago, Illinois, EUA). The samples were immediately sonicated in an ice bath (amplitude 60%, pulse 10 s on/10 s off, 1 min). Next, the sonicated mycelia were centrifuged twice at 4°C and 20,000× *g* for 15 min, and the respective supernatants were carefully collected and stored at -20°C in order to perform the subsequent analyses. Total protein concentration was determined using the Bio-Rad protein assay, based on the Bradford method (Bio-Rad Laboratories, Hercules, California, CA, USA). One-dimensional polyacrylamide gel electrophoresis using 50 μg of intracellular protein extract was performed to validate protein quality.

Finally, for the second-dimension gels and enrichment of phosphopeptides, 300 μg and 100 μg of a mixture of equal concentrations of intracellular proteins was used, respectively, for all time points of sugarcane bagasse culture. The samples were precipitated using 10% tricarboxylic acid (TCA) and incubated in acetone at -20°C overnight. The precipitated proteins were then pelleted by centrifugation at 10,000× *g* for 10 min at 4°C. The pellets were washed three times in 0.07% β-mercaptoethanol and cold acetone. The precipitate was then purified using a 2-D Clean-Up Kit (GE Healthcare, Chicago, Illinois, EUA).

2D-PAGE

Samples were applied to an immobilized pH gradient (IPG)-strip (non-linear 13-cm Immobiline DryStrip pH 3–10 strip, GE Healthcare, Chicago, Illinois, EUA) by in-gel rehydration on IPGbox (GE Healthcare). All isoelectric focusing assays were performed on an Ettan IPGphor 3 IEF system (GE Healthcare, Chicago, Illinois, EUA) at 20°C, with a maximum of 50 μA/strip. The focusing parameters were as follows: rehydration time, 16 h; step 1, 500 V constant for 1 h; step 2, gradient of 1000 V for 1 h; step 3, gradient of 8000 V for 4 h; and step 4, 8000 V for 6 h. Focused strips were equilibrated in two stages with 10 mL of SDS equilibration buffer (6 M urea, 30% (v/v) glycerol, and 2% (w/v) SDS in 50 mM Tris-HCl, pH 8.8, 0.002% bromophenol blue solution). First, the focused proteins were reduced by adding 1% DTT to 10 mL of SDS (equilibration solution) and stirring for 20 min. Then, in the second equilibration stage, the proteins were alkylated with 2.5% iodoacetamide in 10 mL of SDS equilibration solution for 25 min [24]. Equilibrated IPG strips were separated on 12.5% SDS-PAGE gels according to the method described by Laemmli [25] on a SE 600 Ruby system (GE Healthcare, Chicago, Illinois, EUA). Gels were run in buffer (25 mM Tris, 192 mM glycine, pH 8.3, containing 0.1% SDS and traces of bromophenol blue) at a maximum voltage of 600 V, 25 mA, and 2.5 W per gel for 30 min, followed by fixing a maximum voltage of 600 V, 35 mA, and 20 W per gel for 4 h, both sides at 6°C.

Phosphorylated proteins were detected using a fluorescent Pro-Q Diamond Phosphoprotein Gel Stain kit (Molecular Probes, Eugene, OR, USA) according to the standard protocol provided by the manufacturer. Then, the gels were hydrated twice for 5 min with Milli-Q water to acquire the images. Total proteins in the gels were stained overnight with Coomassie Brilliant Blue R-250 (0.25% Coomassie Blue R-250, 50% methanol, and 10% acetic acid), and destained until the appearance of protein in a solution of 30% methanol and 10% acetic acid.

Gels were scanned using a Molecular Imager® PharosFX™ Systems laser scanner at a resolution of 100 μm using the Quantity One software, version 4.6.9 (Bio-Rad Laboratories, Hercules, California, CA, USA). For acquisition of images of the gels stained with the Pro-Q Diamond kit, we used an emission filter at 532 ± 50 nm, while for gels stained with Coomassie blue R-250, we used a white light source without filters. For the analysis, the PDQuest software (Bio-Rad Laboratories, Hercules, California, CA, USA) was used, through which the gels were adjusted in brightness, contrast, and size in order to be standardized. The detection of spots was performed with an automatic matching software, and then all spots in the gel were manually checked to detect possible incorrect detections such as noise, edges of labels, or gels.

Phosphorylation profiling by 2D-PAGE

For identification of phosphoproteins by 2D-PAGE, spots were selected by comparative analysis of images of gels stained with Pro-Q Diamond phosphoprotein gel stain and Coomassie blue R-250. After removal of the dye and SDS, the spot segments were washed three times in a decolorizing solution (50% 100 mM ammonium bicarbonate and 50% acetonitrile) over 24 h under stirring. Immediately after, the spots were submerged in a solution of 100% acetonitrile for 10 min, and completely dried on a SpeedVac Vacuum System (Savant Instrument, Farmingdale, NY, USA). For protein digestion, spots were rehydrated with 20 μL of a 50-mM ammonium bicarbonate solution containing 20 ng μL^{-1} of sequencing-grade modified trypsin (Promega, Madison, WI, USA). After 30 min of rehydration with the trypsin solution, the spot segments were covered with a 50-mM ammonium bicarbonate solution. The hydrolysis reaction was carried out at 37°C for 24 h and then stopped with 50 μL of blocking solution (1% formic acid and 5% acetonitrile). The peptides were extracted with two 30-min washes in wash solution (49.5% acetonitrile and 1% formic acid). The supernatants were dried in the SpeedVac Vacuum System and resuspended in 30 μL of 100% acetonitrile solution. After digestion, peptides were collected using Supel-Tips C18 Pipette Tips (Sigma-Aldrich, St. Louis, MO, USA).

Gel-free phosphoprotein and phosphosite identification

For gel-free identification of phosphorylated proteins and peptides, the proteins were initially solubilized in 8 M urea (1:1), reduced by the addition of a 5-mM DTT solution, and alkylated with 14 mM iodoacetamide. The samples were then diluted in a 50-mM ammonium bicarbonate solution (1:5) and a 1-mM $CaCl_2$ final solution. Trypsin digestion was performed using a 50:1 protein:trypsin ratio (50 μg protein:1 μg trypsin) for 16 h at 37°C. The digestion reaction was stopped with the addition of 0.4% TFA. Digested samples were desalted using a SepPack C18 Vac Cartridge (Waters, Milford, MA, USA). Subsequently, the digested proteins were divided into two groups, one of which was processed with the Phos SpinTrap Fe kit (GE Healthcare, Chicago, Illinois, EUA) to be enriched in phosphorylated peptides. Then, both groups were analyzed by LC-MS/MS using the LTQ Orbitrap XL ETD Hybrid Ion Trap-Orbitrap Mass Spectrometer (Thermo Fisher Scientific, Waltham, MA, USA) coupled with the liquid chromatography EASY-nLC II system (Proxeon Biosystems, Odense, Denmark) through a Proxeon nanoelectrospray ion source. Peptides were separated in a 2–90% acetonitrile gradient in 0.1% formic acid using a PicoFrit analytical column (length, 20 cm; diameter, 75 μm; particle size, 5 μm; New Objective, Littleton, MA, USA). The tension in the nanoelectrospray ion source was 2.2 kV and the source temperature was 275°C. The LTQ Orbitrap Velos workstation (Thermo Fisher Scientific, Waltham, MA, USA) was set in data-dependent acquisition mode. Full-scan MS spectra (m/z 300–1600) were acquired by the Orbitrap analyzer after accumulation to the target value of 1 to 6. The resolution on the Orbitrap analyzer was set to $r = 60{,}000$, and the top 20 peptide ion charge states ≥ 2 were sequentially isolated to the target value of 5,000 and fragmented in the linear ion trap by low-energy collision-induced dissociation (normalized collision energy of 35%). Dynamic exclusion was activated with an exclusion list size of 500, an exclusion list duration of 60 s, and a repeat count of 1. An activation q of 0.25 and a 10-ms activation time were used. For the identification of phosphopeptides and phosphorylated proteins the Mascot software (http://www.matrixscience.com/search_form_select.html) was used, together with the protein database included in the *Trichoderma reesei* 2.0 genome database (https://mycocosm.jgi.doe.gov/Trire2/Trire2.home.html). NetworKIN was used to predict which kinases target specific phosphorylation sites, using criteria according to [26].

Enzymatic assays

β-glucosidase and β-xylosidase activity were assessed as previously described [3,7,27]. Filter paper activity (FPase) was determined by monitoring enzymatic reactions on no. 1 Whatman filter papers (Whatman, Maidstone, UK) with 30 μL of a 100-mM citrate-phosphate buffer at pH 5.0 and 30 μL of sample [28]. Reactions were incubated at 50°C for 30 min. Next, 60 μL of dinitrosalicylic acid (DNS) was added to the reaction, which was then heated at 95°C for 5 min. Carboxymethylcellulase (CMCase) activity was determined following a previously described protocol [29] with some modifications. Briefly, the reaction mixture consisted of 30 μL of 1% carboxymethylcellulose in a 50-mM sodium acetate buffer (pH 5.0) and 30 μL of sample. The reaction underwent incubation at 50°C for 30 min, followed by the addition of 60 μL of DNS, and an additional heating step at 95°C for 5 min. All enzymatic activity assays were performed in 96-well microplates, and absorbance was read at 540 nm (FPase and CMCase activities) and 405 nm (β-glucosidase and β-xylosidase activities) using the xMark™ Microplate Absorbance Spectrophotometer (Bio-Rad Laboratories, Hercules, California, CA, USA). One enzyme unit was defined as the amount of enzyme capable of liberating 1 μmol of reducing sugar per minute [30]. For all enzymatic assays, samples consisting of phosphorylated (P) (crude extract) and unphosphorylated (DP) supernatants were used. Glucose dosage in sugarcane bagasse supernatants was determined using the Glucose Liquiform kit (Labtest Diagnóstica, Lagoa Santa, Brazil) according to the manufacturer's instructions.

Dephosphorylation of the Cel7A enzyme and determination of kinetic parameters

For the dephosphorylation assay of the Cel7A enzyme, the fungi *T. reesei* and *Aspergillus nidulans* were cultivated on sugarcane bagasse. Then, 100 μg of proteins extracted from the supernatant were used for Cel7A (*T. reesei*) and CBHI (*A. nidulans*) purification (Fig. 5C). Purified proteins were then treated with 10 U of FastAP™ Thermosensitive Alkaline Phosphatase (Thermo Fisher Scientific, Waltham, Massachusetts, MA, USA) for 1 h at 37°C. The resultant unphosphorylated samples were used for enzymatic assays to detect Cel7A activity.

Different concentrations of the substrate (4-Nitrophenyl β-D-cellobioside, Sigma-Aldrich, St. Louis, MO, USA) ranging from 0.2 mM to 2 mM were used to determine the kinetic parameters of Cel7A. The reaction mixture consisted of 10 μL of purified Cel7A (treated or not treated with FastAP™ phosphatase), 50 μL of a 50-mM sodium acetate buffer, and 40 μL of substrate. Reactions underwent incubation at 50°C for 3 h, followed by the addition of 100 μL of 1 M sodium carbonate. The enzymatic activity assays were performed in 96-well microplates, and absorbance was read at 405 nm using the xMark™ Microplate Absorbance Spectrophotometer. One enzyme unit was defined as the amount of enzyme capable of liberating 1 μmol of reducing sugar per minute. Reaction rates were measured, and the Michaelis-Menten constant (K_M) and maximum reaction rate (V_{max}) were calculated by fitting the initial reaction rates (v) for each substrate concentration (S) to the Michaelis-Menten equation, using the GraphPad Prism software.

Three-dimensional structure prediction and docking

Three-dimensional models for the proteins of interest were built using the I-TASSER online platform from the Yang Zhang's Research Group (https://zhanglab.dcmb.med.umich.edu/I-TASSER/, version 5.1, University of Michigan, Ann Arbor, Michigan, MI, USA). For this purpose, a FASTA file containing the amino acid sequence of the Cel7A protein was obtained from the UniProt database (protein ID: 123989) and submitted to the I-TASSER online server. The structure modeling approach used by this software is based on the sequence alignment to a protein template, which is identified by LOMETS, a method that selects the top 10 alignments in a PDB library. Then, the unaligned regions of the sequence are built via *ab initio* folding, by considering the lowest free-energy states and minimal sterical clashes identified by SPICKER and TM-align, respectively. The final models are built at the atomic level

by REMO, which optimizes the hydrogen-bonding profile. The I-TASSER online software also enables the prediction of the protein's biological function, since it compares the designed models to different libraries of proteins with already identified functions [31,32]. All predictions, along with the putative ligands provided by the I-TASSER platform, were visualized and configured using the PyMOL Molecular Graphics System (https://pymol.org/2/, version 1.8.6.0, Schrödinger LLC, New York, NY, USA).

The docking analysis was performed using AutoDock 4.2 on the graphical user interface AutoDockTools (ADT) [33], using the step-by-step protocol published by Rizvi et al. (2013) [34]. AutoDock quantifies the enthalpic and entropic contributions using an approach of a semiempirical free energy force field, which measure the biding energy between two or more molecules. Therefore, the free binding energy corresponds to the difference between the energy of the unbound ligand and protein, and the energy of the ligand-protein complex [35]. For this purpose, the program considers dispersion/repulsion, hydrogen bonding, electrostatics, and desolvation, as well an estimative of the conformational entropy lost upon binding. The search parameters used were those of the Genetic Algorithm with Lamarckian GA output, in default configurations. Cellulose was designed with ACD/ChemSketch version 2019.2.1 (Advanced Chemistry Development, Inc., Toronto, ON, Canada, www.acdlabs.com).

Results

Enzymatic activity

In order to establish the dynamics of holocellulase production over time, *T. reesei* was cultivated for 24, 48, 72, and 96 h on sugarcane bagasse, and glucose release and extracellular cellulase activity were measured. Maximum cellulase activity and glucose release were detected at 96 h (Fig. 1A). However, as shown in Fig. 1A, enzymatic activity was detected already after 24 h of growth. Therefore, the goal of this work was to identify phosphorylation sites related to different phosphorylation events. For this purpose, the culture supernatants for all of the abovementioned cultivation time points were mixed and used as protein pool for further experiments.

Quantitative phosphoproteomic analysis

To identify phosphorylated proteins, we first performed 2D-PAGE in order to obtain an overview of the number of proteins that were phosphorylated when *T. reesei* was cultivated in the presence of sugarcane bagasse (a scheme of the methodology is summarized in Fig. 2). In this analysis, a total of 45 spots were detected automatically by the software PDQuest (Bio-Rad) from gels stained with colloidal Coomassie and gels subjected to the Pro-Q Diamond reagent from three biological replicates,

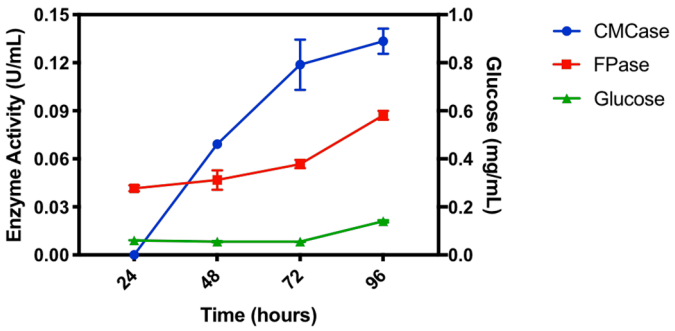

Fig. 2. Workflow for the identification of the *T. reesei* phosphoproteome.

as illustrated in (Fig. S1 and Supplementary Table S1). To overcome 2D-PAGE gel-to-gel variance, we also used gel-free analysis comparing samples from SBC and glucose conditions for an overview of the *T. reesei* phosphoproteome during sugarcane bagasse degradation. In order to obtain more accurate results, we used the data obtained from total proteomics to filter the phosphoproteomics data. Therefore, only the phosphorylated proteins that had also been identified in the proteome were considered for further analysis. The Fig. 1B shows the Venn diagram with only 8 proteins shared by SCB and glucose conditions, indicating specific mechanism to response to holocellulases inducing conditions (SCB) and repressing condition (glucose). Moreover, among the proteins commonly identified in the two conditions, 5 are involved with energy metabolism and 3 are unknown or not predicted.

Concerning to SCB, a total of 255 unique phosphopeptides from 114 proteins were identified in at least two biological replicates (Fig. 1B). Phosphoserine and phosphothreonine (Ser, Thr) corresponded to the 90% of the phosphosites while 10% of them were related to phosphotyrosine (Tyr) (Fig. 3A, Table 1). Among the identified proteins, 65% were singly phosphorylated, 19% were doubly phosphorylated, 12% were triply phosphorylated, and 4% were more than triply phosphorylated, including one peptide that presented 11 phosphosites (Fig. 3A). All the identified peptides were subjected to prediction for enrichment in any specific motif by Motif-X. However, peptides were found not to be enriched in any motif. On the other hand, when all phosphosites were analyzed by NetworKIN 3.0, it was possible to identify kinases that could recognize and phosphorylate the detected phosphosites (Fig. 3B). In particular, after applying the NetworKIN filtering criteria (STRING score $\geq$ 0.6 and NetworKIN score $\geq$ 1.0), 75 kinases were predicted to phosphorylate the sites identified in this work, including 19 serine/threonine kinase families putatively targeting all identified phosphorylation sites. The most frequently predicted serine/threonine kinase was PKC1, followed by SNF1, AKL1, and RAD53. Interestingly, our phosphorylome data was also enriched in casein kinases (CK1 and CK2), which have

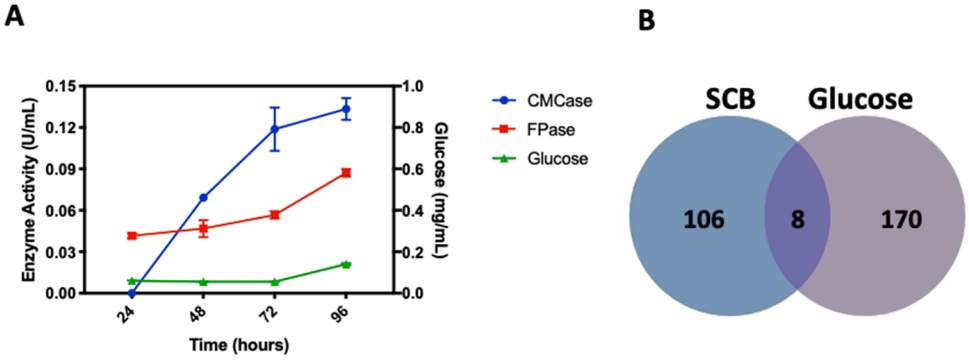

Fig. 1. Cellulolytic activity and glucose releasing of *T. reesei* cultivated in the presence of sugarcane bagasse for the indicated times. (A) Enzymatic activity of *T. reesei* using CMC and Filter Paper (FP) as substrates. (B) Venn Diagram of phosphoproteins identified from sugarcane bagasse (SCB) and glucose conditions. These results are based on three replicates for three independent experiments and are expressed as mean ± standard deviation.

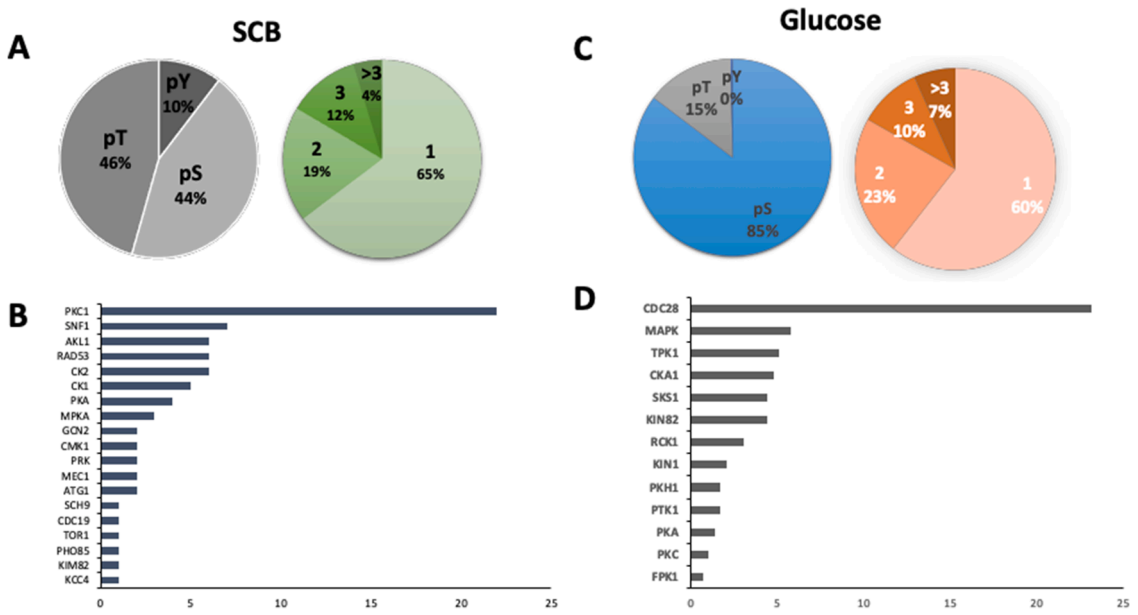

Fig. 3. Phosphorylation profiling of *T. reesei* cultivated in the presence of sugarcane bagasse (A and B) and glucose (C and D) conditions. (A) and (C) Distribution of phospho-Ser (pS), phospho-Thr (pT), and phospho-Tyr (pY) residues and distribution of peptides with single, double, triple, or more phosphorylation sites are shown. (B) and (D) Prediction of major kinases responsible for phosphorylating the identified proteins in the phosphoproteomics.

been suggested to be important regulators of phosphorylation events in filamentous fungi.

On the other hand, in presence of glucose as carbon source, a total of 348 unique phosphopeptides from 170 proteins were identified in at least two biological replicates (Fig. 3B and Supplementary Table S2). Phosphoserine and phosphothreonine (Ser, Thr) corresponded almost to 100% of the phosphosites while 0.89 % of them were related to phosphotyrosine (Tyr) (Fig. 3C, Supplementary Table S2). Among the identified proteins, 60% were singly phosphorylated, 23% were doubly phosphorylated, 10% were triply phosphorylated, and 10% were more than triply phosphorylated (Fig. 3C). Furthermore, when all phosphosites were analyzed by NetworKIN 3.0, it was possible to identify kinases that could recognize and phosphorylate the detected phosphosites (Fig. 3D), using the same criteria as before.

Considering the growth in glucose as sole carbon source, we were able to identify 13 different groups of kinases responsible for protein phosphorylation in this circumstance, whereas CDC28 was the most prevalent group found, followed by MAPK, TPK1, CKA1, SKS1, KIN82 and others (Fig. 3D). The most numerous kinase from the CDC28 group found here was a Pho85-like protein, being a cyclin-dependent kinase (CDK) that is highly related to PHOA, which is responsible for sexual differentiation and cell development in *Aspergillus nidulans* [36]. We also found a high amount of MAPK, which are responsible for the regulation of cellulases production and osmolarity, cell wall maintenance and sporulation in *T. reesei* [20,37]. TPK1, a PKA catalytic subunit, was responsible for the phosphorylation of several phosphosites as well, being associated to the inhibition of filamentous growth in yeast [38]. Other kinases found were mostly related to the regulation of polarized growth [39] and glucose response [40], among other functions. Together, our data indicate that *T. reesei* uses different phosphorylation pathways to regulate gene expression in response to inducing and repressing carbon sources.

In order to identify physical and functional interactions among the phosphoproteins from SCB highlighted in this work, we used protein interaction information from the STRING database to generate protein interaction networks (Fig. 4). In total, 100 phosphoproteins and 169 edges were mapped (Supplementary Table S3). A global phosphoprotein interaction network was generated by STRING with four proteins related to fatty acid synthesis, five to proteasome, 12 to translation, seven to ribosome, nine to acetyl-CoA metabolism, 12 to carbohydrate metabolism, and six to cysteine and methionine metabolism (Fig. 4).

Effect of phosphorylation on the activity of secreted glycosyl hydrolases

Among the phosphorylated proteins identified in this work, there were four glycosyl hydrolases: a β-xylosidase, Cel7A, a β-glucanase, and a glucuronidase (Table 1). Since these enzymes are known to be secreted, we performed a test to verify the effect of phosphorylation on their enzymatic activities. Therefore, culture supernatants were treated with phosphatase, and subsequently FPase, β-xylosidase, and β-glucosidase activities were measured.

Notably, dephosphorylated enzymes showed ~25% lower FPase activity compared to the control, while β-xylosidase and β-glucosidase activities increased in the dephosphorylated crude extract (Fig. 5A), indicating that post-translational phosphorylation can regulate holocellulases in a different manner. In order to verify the phosphorylation effect in a pure enzyme, Cel7A was purified and treated with phosphatase to test for activity changes. The FPase activity of dephosphorylated Cel7A was about 60% lower than that of the control (Fig. 5B). Moreover, CBHI from *Aspergillus nidulans* was also tested for the effect of phosphorylation on its activity, which resulted very similar to that on Cel7A from *T. reesei*. To study the effect of Cel7A dephosphorylation more in detail, the kinetic constants of phosphorylated and dephosphorylated Cel7A were measured (Fig. 6A).

The comparison of kinetic parameters of phosphorylated and dephosphorylated enzymes revealed interesting features. As demonstrated in Fig. 6A, Cel7ADP (dephosphorylated enzyme) exhibited a decrease in substrate affinity, denoted by a ~2-fold higher K_M value when compared to Cel7AP (phosphorylated enzyme). However, Cel7ADP showed no difference ($P > 0.05$) in turnover number (K_{cat}) with respect to Cel7AP. Conversely, Cel7AP displayed both high substrate affinity and increased catalytic efficiency (K_{cat}/K_M) compared to Cel7ADP (Fig. 6A). These results suggested that phosphorylation may not occur at the catalytic site. Indeed, the phosphosites identified in our phosphorylome (highlighted in red) are located in a region close to the substrate entrance structural sequence (Fig. 6B). Thus, the regulation of glycosyl hydrolase activity by phosphorylation could be an intriguing mechanism for controlling cellulase activity in *T. reesei*. Moreover, our

Table 1
Phosphoproteins identified in presence of sugarcane bagasse by LC-MS/MS.

Protein ID	Protein description	Function	Score	Total peptides	Unique peptides	MW (Da)	Phosphosites
121255	2-methylcitrate dehydratase-like protein	2-methylcitrate dehydratase activity	85	13	2	60,262	268/270
122301	Cystathionine beta-lyases/cystathionine gamma-synthases	amino acid metabolism	35	4	2	46,594	219/359
75689	Arginyl-tRNA ligase.	arginyl-tRNA aminoacylation	44	8	2	76,272	127/504/505/513/617
55362	Heat shock protein 70	ATP binding	505	36	20	73,565	525
71363	translation elongation factor 3-like protein	ATP binding	95	9	3	116,987	348/505/509
80142	HSP104 and related ATP-dependent Clp proteases	ATP binding	99	13	4	103,180	363/365
82534	heat shock protein (Hsp70 chaperone Hsp88)	ATP binding	105	9	3	79,313	36/38/555
120053	Hsp70 family protein	ATP binding	78	15	4	73,111	385
122572	hsp70 family protein	ATP binding	62	10	4	66,812	118/317/507/509
122920	Molecular chaperone Bip	ATP binding	202	14	7	72,660	637/644
51499	ketol-acid reductoisomerase, mitochondrial precursor	branched chain family amino acid biosynthesis	118	12	4	44,920	ND
56920	Leucine aminopeptidase 1	calcium ion binding	35	5	1	43,659	133/134
120198	glycosyl transferase, family 35, glycogen phosphorylase 1	carbohydrate metabolism	118	7	4	100,868	42
121127	GH3 β-xylosidase BXL1	carbohydrate metabolism	240	18	9	87,479	553/653
123026	transaldolase	carbohydrate metabolism	206	16	9	35,698	ND
21957	pyruvate carboxylase (cytosolic)	catalytic activity	46	14	3	131,844	40
107784	ribosomal protein L18ae	cellulose binding	148	8	4	20,679	110/122
47221	Nucleoside diphosphate kinase	CTP biosynthesis	50	9	3	16,991	99
81089	CysK, Cysteine synthase; aa370-414 cd02205, CBS domain	cysteine biosynthesis from serine	62	11	2	55,118	196/201/292
2537	RHO protein GDP dissociation inhibitor	cytoplasm	33	7	2	22,283	13/71/151
45138	sulfite reductase, ß-subunit	electron transport	226	19	7	168,869	270/271/274/275
23171	NRPS	fatty acid biosynthesis	18	165	1	2,314,768	7447/7448/13790/ 13791/20474/13769/ 4718/17468/1935/ 15914/10770/2902/ 2907/14180/7141/7143/ 7144/7149
77656	phosphoglycerate mutase	fatty acid biosynthesis	63	6	1	58,658	4/504/518
121661	aldose-1-epimerase	galactose metabolism	202	8	6	37,280	95
123114	Heat shock protein 90	galactose metabolism	322	16	11	78,614	585
121420	glutamyl-tRNA synthetase, class Ic.	glutamyl-tRNA aminoacylation	30	8	1	72,637	296/305/306/533
44529	glycogen synthase involved in carbohydrate transport and metabolism	glycogen biosynthesis	30	9	1	81,166	31/359/361/648
5776	glucose-6-phosphate isomerase	glycolysis	120	7	2	60,845	190/195
22994	AAA-ATPase Cdc48	glycolysis	390	27	15	90,046	363/624/632
78439	pyruvate kinase	glycolysis	37	9	1	59,307	5/400
120568	enolase	glycolysis	259	21	9	47,400	4
120235	Elongation factor 2	GTP binding	401	32	15	93,544	76/299
123071	ATP synthase beta chain, mitochondrial precursor, associated to cellulase signal transduction (PMID: 15288024)	hydrogen-transporting ATPase activity, rotational mechanism	76	10	4	54,898	231/238
77336	aconitate hydratase	hydro-lyase activity	203	25	8	86,254	14
120877	Zn-dependent ß-lactamase	hydroxyacylglutathione hydrolase activity	53	7	2	34,005	2/3
59771	UbiA prenyltransferase, putative	integral to membrane	72	35	9	35,189	220
59346	chitin biosynthesis protein CHS5	intracellular	34	7	1	43,167	172
120779	unknown protein	intracellular	26	3	1	23,299	157
21836	phosphoglucomutase/phosphomannomutase	intramolecular transferase activity, phosphotransferases	87	9	3	60,244	ND
65295	Serine hydroxymethyltransferase	L-serine metabolism	14	2	0	54,488	190
77481	D-xylulose 5-phosphate/D-fructose 6-phosphate phosphoketolase	lyase activity	118	14	5	92,235	30
67541	MFS permease	membrane	20	34	5	60,300	273/274/278/381
4117	alpha-aminoadipate reductase lys2	metabolism	84	11	1	128,765	670/676/747
120675	ArgE	metallopeptidase activity	197	15	8	52,540	421
119735	Glyceraldehyde-3-phosphate dehydrogenase, isozyme 2	NAD binding	97	11	4	36,361	187
79686	Unknown protein with RNA binding domains	nucleic acid binding	65	11	1	81,311	5/6/7/25
80200	transcription factor (Snd1/p100)	nucleic acid binding	74	9	2	97,989	205/206/209/212
120535	unknown protein	nucleic acid binding	36	2	1	23,071	181
43664	UTP-glucose-1-phosphate uridylyltransferase	nucleotidyltransferase activity	104	12	4	57,908	ND
121989	oxalate decarboxylase	nutrient reservoir activity	107	5	4	50,251	114
110171	S-adenosyl-L-homocysteine hydrolase	one-carbon compound metabolism	156	16	8	48,908	2/245/332/335
53567	glutathione reductase	oxidoreductase activity	38	5	3	51,193	390/393/396/408/409
74194	mannitol dehydrogenase LXR1	oxidoreductase activity	46	5	2	28,631	157/159/173
74983	Isocitrate dehydrogenase, subunit 2, NAD-dependent, mitochondrial	oxidoreductase activity	21	6	1	41,229	223

(*continued on next page*)

Table 1 (*continued*)

Protein ID	Protein description	Function	Score	Total peptides	Unique peptides	MW (Da)	Phosphosites
80920	ADH1	oxidoreductase activity	62	9	3	38,151	226/228
81303	fumarate reductase	oxidoreductase activity	48	8	2	67,143	532
81576	Assimilatory sulfite reductase,Alpha subunit	oxidoreductase activity	27	14	2	115,265	ND
107776	xylose reductase	oxidoreductase activity	273	12	6	36,713	143
120943	NAD-dependent glutamate dehydrogenase	oxidoreductase activity	134	13	5	120,067	23/53/695/696
122778	short chain dehydrogenase/reductase	oxidoreductase activity	44	4	1	35,927	ND
123729	malate dehydrogenase	oxidoreductase activity	373	13	10	35,233	14/2238
123946	dehydrogenase associated with cellulase signal transduction (PMID: 15288024)	oxidoreductase activity	43	6	1	31,952	40/295
123989	GH7 Cellobiohydrolase CBH1/Cel7A	oxidoreductase activity	144	5	4	55,445	95/99/104/107/109
50531	2-oxoglutarate dehydrogenase-like protein	oxidoreductase activity, acting on the aldehyde or oxo group of donors, disulfide as acceptor	39	11	2	117,609	789
58073	uroporphyrinogen decarboxylase	porphyrin biosynthesis	58	6	2	40,917	344
77330	26S proteasome regulatory complex subunit Rpn9	proteasome endopeptidase activity	33	2	1	43,557	147/165/166
44504	actin	protein binding	30	3	1	41,823	300
62820	Ribosomal protein(60S) L152/L15B	protein biosynthesis	99	6	3	24,210	165/167
74568	unknown protein	protein biosynthesis	55	11	3	29,490	105
76939	Ribosomal protein S9, S4 family	protein biosynthesis	40	4	2	22,125	143
49213	14-3-3 protein	protein domain specific binding	194	9	7	30,520	3
120044	GDP dissociation inhibitor Gdi1	protein transport	109	10	3	51,575	ND
51365	Subtilisin-like protease PPRC1	proteolysis and peptidolysis	100	8	3	93,779	710
77579	aspartyl protease	proteolysis and peptidolysis	86	5	1	42,632	328/330
81517	unknown protein	proteolysis and peptidolysis	35	19	1	154,792	688/689/754/755/962/963/1295
108592	unknown protein	proteolysis and peptidolysis	61	5	2	68,495	8/13
121298	formate dehydrogenase	proteolysis and peptidolysis	72	5	3	40,822	314/316/317
123244	Serine proteinase Sub8	proteolysis and peptidolysis	146	12	4	58,343	ND
121534	pyruvate decarboxylase	pyruvate decarboxylase activity	34	5	1	63,479	ND
78423	26S proteasome regulatory complex subunit Rpn2	regulation of cell cycle	42	9	1	122,774	126/127/133/134/135/187
76215	sulfide:quinone oxidoreductase/flavo-binding protein	regulation of oxidoreductase activity	63	6	1	48,761	233/349/350
123827	bifunctional catalase/peroxidase	response to oxidative stress	210	16	9	83,056	18/229
123631	Saccharopine dehydrogenase	saccharopine dehydrogenase (NADP+, L-glutamate-forming) activity	30	5	1	49,109	375/376/377/389/393/439
76247	O-methyltransferase family protein	S-adenosylmethionine-dependent methyltransferase activity	168	6	5	26,953	13
78591	fatty acid synthase beta subunit [Includes: 3-hydroxypalmitoyl-[acyl-carrier-protein] dehydratase;Enoyl-[acyl-carrier-protein] reductase [NADH];[Acyl-carrier-protein] acetyltransferase; [Acyl-carrier-protein] malonyltransferase; S-acyl fatty	transferase activity	25	26	1	233,292	2/4/6/10/308/330/992/1662/1881/1883/1884
72012	GT8 glycogenin	transferase activity, transferring hexosyl groups	65	6	1	61,317	284
120635	transketolase-like protein	transketolase activity	167	15	7	75,622	620
123902	elongation factor 1, gamma chain.	translational elongation	258	14	9	45,926	ND
121901	eukaryotic translation initiation factor 3 subunit 8, N-terminal.	translational initiation	24	9	1	98,188	310
72606	ubiquitin-activating enzyme UBA1	ubiquitin cycle	76	8	1	115,535	50/670/673/876
66707	20S proteasome beta-type subunit Pre3	ubiquitin-dependent protein catabolism	80	4	3	23,253	144/145/148/150
76010	20S proteasome, alpha subunit Pre6	ubiquitin-dependent protein catabolism	65	4	2	29,909	115
121343	20S proteasome alpha-type subunit Pre5	ubiquitin-dependent protein catabolism	59	5	1	29,965	ND
121820	Methionine_syntMethionine synthasevitamin-B independent	unfolded protein binding	429	25	14	85,849	287/290/328/329/330
80843	26S proteasome regulatory complex subunit Rpn8	zinc ion binding	46	4	1	38,289	4/13
21509	blue light inducible protein BLI-3	ND	46	5	2	22,602	ND
40538	unknown protein	ND	26	34	3	25,091	59
54674	unknown protein	ND	19	12	1	64,653	25/28/35/37/155/202/203/206
59940	unknown protein	ND	34	4	1	24,556	139/217
62100	Hsp30	ND	514	21	16	23,126	97
67616	unknown protein	ND	34	5	1	29,849	177
75424	Mitochondrial Matrix Factor	ND	66	8	2	13,763	71
76366	NADH:flavin oxidoreductase/12-oxophytodienoate reductase	ND	74	5	2	49,952	372
78242	unknown protein	ND	114	2	1	56,256	193
78401	unknown protein	ND	222	32	13	118,769	

(*continued on next page*)

Table 1 (*continued*)

Protein ID	Protein description	Function	Score	Total peptides	Unique peptides	MW (Da)	Phosphosites
							11/154/434/435/436/706/707/710/715/805/1063/1065
79606	GH115 xylan- α-1,2-glucuronidase or α-(4-O-methyl)-glucuronidase	ND	40	8	1	112,649	ND
80437	unknown protein	ND	20	24	1	42,292	51/52/53/60
82599	unknown protein	ND	20	5	1	86,334	3/11
105156	unique protein	ND	45	5	2	33,290	146/153
106982	unknown protein	ND	23	34	4	40,277	14/250/279/283
109282	unknown protein	ND	47	5	1	39,379	270
121717	unknown protein	ND	94	4	2	18,046	ND
121746	GH55 exo-1 3-β-glucanase GLUC78	ND	63	4	2	83,604	8
122696	unknown protein	ND	43	9	1	57,824	212/450

ND – Not Determined.

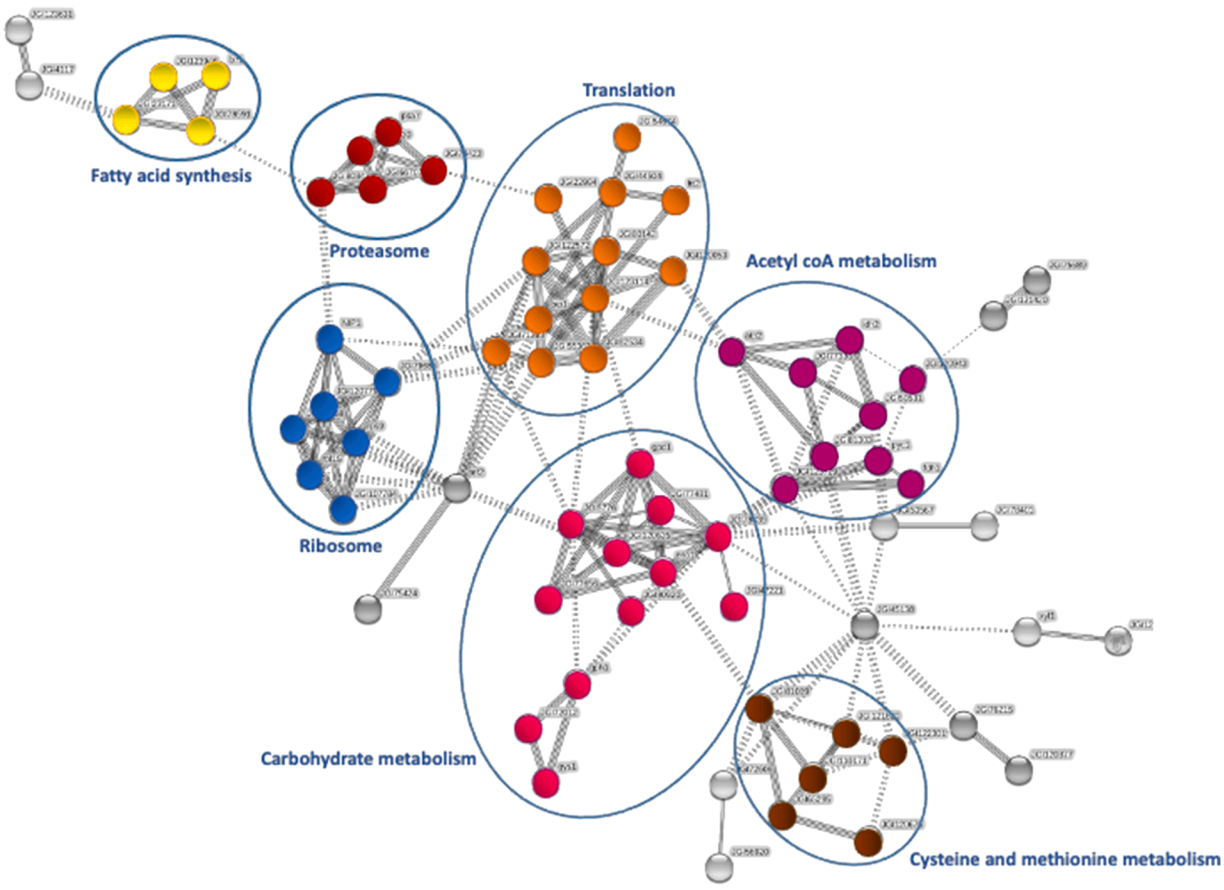

Fig. 4. Protein-protein interaction network of phosphorylated proteins identified in sugarcane bagasse condition. The interaction network contains 100 nodes and 169 edges, as found by STRING.

results suggest for the first time the occurrence of this kind of regulation in this fungus.

Predicted three-dimensional structures and docking of Cel7A

Among the enzymes that degrade sugarcane bagasse, some proteins of the Carbohydrate-Active enZyme (CAZymes, http://www.cazy.org/) family were identified, which display several phosphorylation sites throughout their sequences. In this context, the Cel7A protein was chosen because of its importance in the degradation of biomass. In order to confirm the possible phosphorylation sites, the I-TASSER online platform from the Yang Zhang's Research Group was used [31,32]. The template used was the crystalized structure of Cel7A from *T. reesei* (PDB: 6CEL, chain A), resolved by Divne et al. [41], and the model obtained presented a C-score of 0.80, a TM-score of 0.6 ± 0.14, and a root mean square deviation (RMSD) of 9.2 ± 4.6 Å. These results validated the model proposed for non-bounded Cel7A. In order to simulate the phosphorylated form of Cel7A, we edited its FASTA sequence by a change of the amino acids Ser, Thr, and Tyr into Glu and Phe, the Ser/Tyr residues in the phosphosites identified by the phosphoproteome were mutated to Phe or to phosphomimetic Glu (Supplementary material 1-4). According to Silveira et al. (2018), the Cel7A binding site comprises a set of β-sheets surrounded by loops and helices that form a tunnel for the entry of a sole glucan chain, for its efficient hydrolysis [42]. The Fig. 7 shows the conformational changes in the structure of models, in the phosphomimetic model the CDB displays a

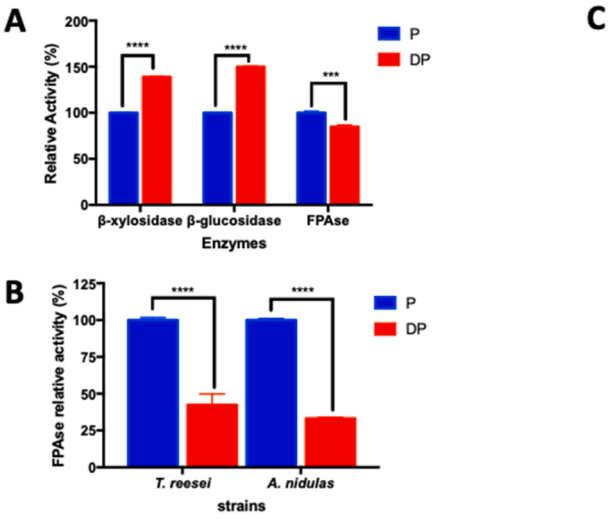

Fig. 5. Effects of phosphorylation on the holocellulolytic activity of *T. reesei.* (A) Cellulolytic activities of the crude extract upon incubation with phosphatase (dephosphorylated, DP) and the control (no treatment, phosphorylated, P). (B) FPase activity of Cel7A (*T. reesei*) and CBHI (*A. nidulans*) purified and upon treatment with phosphatase (DP) and the control (no treatment, P). (C) SDS-PAGE gel with Cel7A and CBHI enzymes purified from the supernatant of *T. reesei* and *A. nidulans,* respectively, in cultures of sugarcane bagasse.

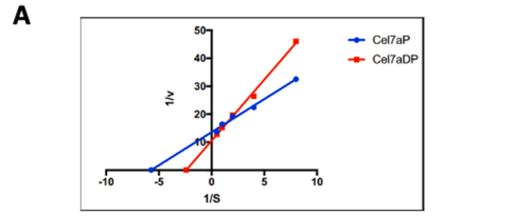

Enzyme	Kcat (s^{-1})	K_M (mM)	Kcat/K_M (mM^{-1} s^{-1})
Cel7aP	0.076 ± 0.009	0.196 ± 0.036	0.388 ± 0.011
Cel7aDP	0.092 ± 0.007^{ns}	0.391 ± 0.027	0.236 ± 0.074

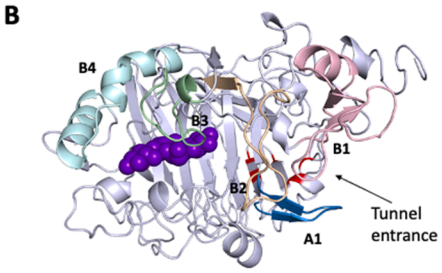

Fig. 6. Kinetic parameters and predicted three-dimensional structures of Cel7A. (A) Lineweaver-Burk plot for the determination of kinetic parameters for native (blue) and dephosphorylated (red) Cel7A. The table shows the calculated values for the parameters in each condition. (B) Predicted three-dimensional structures of Cel7A. The regions of the protein highlighted in red represent the phosphosites identified by MS Orbitrap. Region B1 is highlighted in light pink, A1 in blue, B2 in orange, B3 in light green, and B4 in cyan.

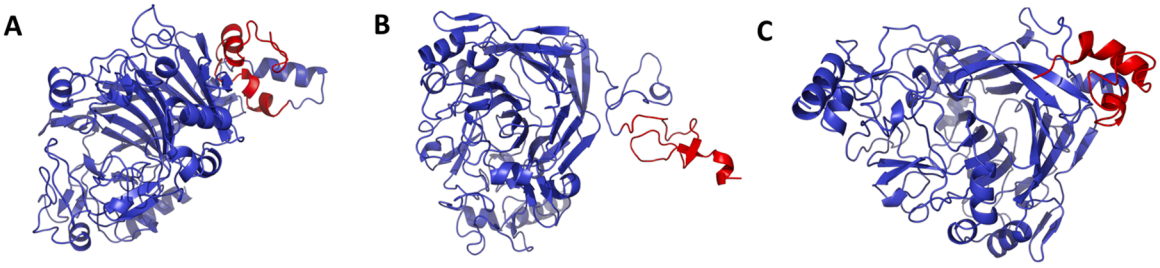

Fig. 7. Predicted three-dimensional structures of Cel7A showing conformational changes in CBD (in red). (A) Wild type Cel7a, (B) Phosphorylated Cel7a and (C) Non-phosphorylated Cel7a.

stereochemical configuration more favorable to interaction with the substrate, when compared to the structure of the wild-type and dephosphorylated protein models.

Therefore, phosphorylation seems to be important for the recognition or positioning of the substrate at the active site of Cel7A. The presence of different phosphosites on the Cel7A structure supports the results of our enzymatic assay and reinforces the hypothesis that phosphorylation is an important regulatory mechanism in *T. reesei*. In the Fig. 8C, when analyzing the superposition of the two modeled structures (natural-state Cel7A bound to the cellulose fiber - Fig. 8A, and Phosphorylated Cel7A (amino acid mimics) bound to cellulose - Fig. 8B), it was possible to notice changes not only near the known phosphosites, but also in the cellulose-binding domain (CBD) of Cel7A. We believe that phosphorylation of these phosphosites allows a global change in the overall structure of Cel7A, interfering with the recognition of the cellulose chain by its CBD. This conclusion is also supported by the docking analysis we performed to assess differences in the affinity for the substrate. In fact, we verified that phosphorylated Cel7A presents more binding affinity to cellulose than the non-phosphorylated enzyme, with binding energies of 3.49×10^7 kcal mol^{-1} and 3.75×10^7 kcal mol^{-1}, respectively. Moreover, phosphorylation allowed the formation of more hydrogen bonds between the protein and the cellulose chain, with three hydrogen bonds formed in the dephosphorylated state against the five formed by the phosphorylated form of Cel7A. These results showed that the phosphorylated form of Cel7A presents higher affinity to cellulose and binds more tightly to it than the natural-state Cel7A.

Discussion

Phosphorylation events in cells may have different functions [10, 43–46]. In fact, phosphorylation may, among others, mark the protein for a specific cellular localization, switch the protein activity on or off, or activate signaling networks [47,48]. Although the importance of phosphorylation is widely acknowledged, some phosphorylation-related

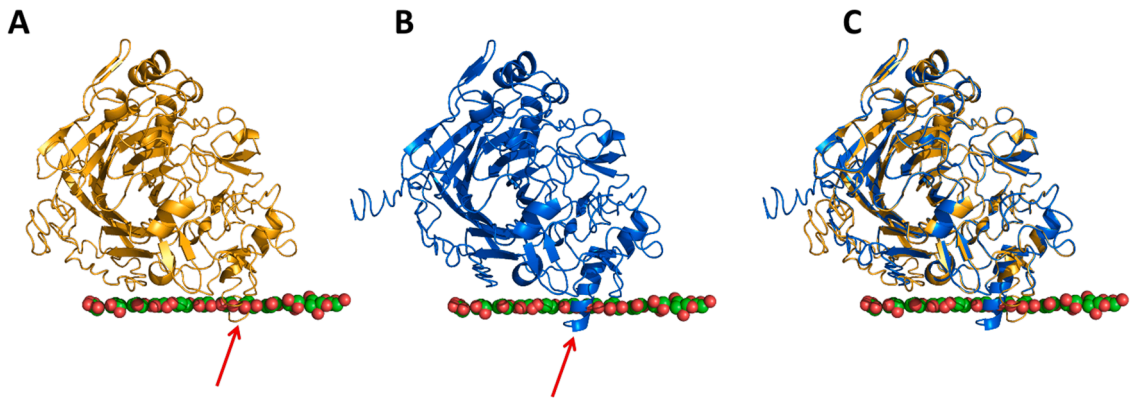

Fig. 8. Predicted structural differences between CBDs from natural-state and phosphorylated Cel7A during cellulose fiber interaction. The phosphorylation of the indicated residues not only provokes conformational alterations around the residues themselves, but globally affects the structure of the CBD. (A) Model of natural-state Cel7A bound to the cellulose fiber. (B) Phosphorylated Cel7A (amino acid mimics) bound to cellulose. (C) Alignment of both enzyme states showing the differences in their conformations. Red arrows shows different conformation in CBD.

signaling networks, as well as the mechanisms of phosphorylation-dependent activation/deactivation of many transcription factors and other proteins, have not been well elucidated. Moreover, in *T. reesei*, a filamentous fungus producing holocellulases, several regulation processes are not well understood, especially when this fungus uses a complex carbon source for its growth. Thus, this work sought to identify all the proteins that are differentially phosphorylated when *T. reesei* is cultivated on sugarcane bagasse, a complex carbon source that has been reported to induce the production of holocellulases, when compared to glucose [20,49–52].

In *T. reesei*, the role of phosphorylation in the regulation of holocellulase gene expression has been explored [37,53,54]. However, none of the previous studies has identified the specific targets or kinases/phosphatases that control the regulatory mechanisms related to holocellulase gene expression. Nevertheless, global transcriptional analysis of two *MAPK* mutants showed that this signaling pathway may control diverse processes in *T. reesei*, such as carbohydrate metabolism, cell growth, development, expression of transporters and epigenetic regulators, and holocellulase gene expression in response to sugarcane bagasse [20]. In this context, our analysis of putative phosphosites showed that serine/threonine MAPK was the eighth most abundant family of kinases suggested to control *T. reesei* phosphorylome in response to sugarcane bagasse. This result highlights the essential role of the MAPK signaling pathway in this fungus. On the other hand, in presence of glucose, a kinase CDC28 was prevalent in phosphorylation of phosphosites targets identified in this study. CDC28 is cyclin-dependent kinases (CDKs) well studied in yeasts such *Saccharomyces cerevisiae, Candida albicans* and *Cryptococcus neoformans* and is involved in vegetative growth and cell cycle regulation [55,56]. CDC28 was not yet characterized in *T. reesei*, but in others filamentous fungi is reported to be involved in cell cycle progression [57].

Moreover, our phosphoproteomic analysis showed that a total of 255 phosphopeptides from 114 proteins were differentially phosphorylated in *T. reesei* grown in the presence of sugarcane bagasse. Phosphorylation at Thr was detected a little more often than at Ser, in contrast with the literature [12,58]. Therefore, we hypothesize that the use of sugarcane bagasse resulted in the activation of still not well-known fungal pathways and thus in the preferential phosphorylation of Thr. The NetworKIN-based prediction of kinases responsible for phosphorylating all the phosphosites identified in this study pointed to PKC1 as the main kinase, followed by SNF1, AKL1, and RAD53. Likewise, PKA represents another prominent kinase in the protein interaction network. This protein is a target of the cAMP-activated signaling pathway and, in turn, regulates by target-specific phosphorylation the function of numerous target proteins including factors that bind to DNA motifs within the promoter regions of cAMP-inducible genes, thereby modulating growth, spore germination, virulence, expression of endoglucanases, and circadian clock in various fungi, including *T. reesei*.

In *Aspergillus fumigatus*, the phosphorylation of PkaR is essential for hyphal growth and cell wall integrity, highlighting that specific phosphorylation by PKA governs numerous processes in fungi [59]. Notably, different studies have indicated the existence of a relationship between the signaling pathway activated by PKA and the carbon source used by fungi [60,61]. In addition, in the presence of light, *T. reesei* PKAC1 (protein kinase A catalytic subunit 1) and ACY1 (adenylate cyclase 1) have been shown to regulate cellulase expression [62].

Consistently, our data suggested that *T. reesei* growth in the presence of sugarcane bagasse can determine the phosphorylation status of different regulatory proteins, which promote specific regulation of target genes in order to control the breakdown of complex carbon sources such as sugarcane bagasse. Interestingly, alterations in the carbon source composition completely change the phosphoproteomic profile of the thermophilic archaeon *Sulfolobus solfataricus* in response to glucose or tryptone [63]. In this organism, sugar metabolism was suggested to be regulated by phosphorylation/dephosphorylation of specific enzymes of different metabolic routes. Altogether, these findings suggest the presence of a finely tuned and specific regulation of signaling pathways controlling carbon source utilization. This information is extremely important for a better understanding of the signaling pathways that are preferentially activated when *T. reesei* uses complex carbon sources. Furthermore, our protein interaction networks highlighted the importance of phosphorylation events in the regulation of cellular growth and development when the fungus senses a complex carbon source, such as sugarcane bagasse.

One of the identified phosphorylated proteins was cellobiohydrolase (Cel7A), the protein most secreted by *T. reesei* [64,65]. This is the main enzyme responsible for cellulose degradation by this fungus, but there was no previous report of its phosphorylation at any site. Therefore, our results allowed the first identification of Cel7A phosphorylation sites and suggested that phosphorylation may be important for regulating the activity of this protein. When Cel7A purified from culture broth (i.e., secreted) was dephosphorylated, it showed a lower activity compared to its native counterpart. This result suggests that phosphorylation of Cel7A plays an important role in regulating its activity once it is secreted. Moreover, kinetic analysis suggested that dephosphorylation decreases Cel7A affinity for its substrate, and molecular modeling of the phosphosites on the structure of this enzyme supports this hypothesis by showing these sites along the substrate entrance site of Cel7A.

It has been suggested that Cel7A presents an open and a closed state: the first mediates the hydrolysis of cellulose through its affinity for reducing and non-reducing ends, whereas the latter enables the substrate to reach the active site through the tunnel entrance [42]. The

tunnel is composed of loops and helices that allow the enzyme to close and hydrolyze the glucan polymer as a single chain [66]. We suggest that the phosphosites found near the A1 and B1 regions of the tunnel may affect the conformational changes mediating the switch between opened and closed state, thereby interfering with the way the enzyme initiates cellulose hydrolysis, or even with the entry of the substrate in the tunnel so that it can be hydrolyzed. In summary, this is the first report of Cel7A phosphorylation and how this modulates its activity.

In our study, from the differential molecular modeling of dephosphorylated Cel7A and its phosphorylated form (through amino acid mimics), we could notice not only local changes around the highlighted phosphosites, but also global changes in the overall structure, especially in the CBD. Therefore, local changes might activate or repress cellulase hydrolysis by altering the way the cellulose fiber interacts and binds to the active tunnel at the CBD. In addition, we suggest that conformational changes in the CBD, mediated by the phosphorylation of its surrounding amino acids, might affect Cel7A recognition and attachment to cellulose. Indeed, phosphorylation may not only modulate the strength of interactions or change the binding energy for a preferred conformation, but also change the recognition patterns of a protein, thus disrupting protein complexes [67–69].

Cellulose hydrolysis by *T. reesei* involves sequential steps, such as enzyme adsorption to the cellulose surface, formation of a complex between the catalytic domain (CD) and the cellulose reducing end, entry of cellulose into the catalytic tunnel for the hydrolysis itself, decomplexation, and detachment of the enzyme. The recognition and the attachment to the cellulose fiber by the CBD of the enzyme are crucial for the complexation of the CD with cellulose and, thus, cellulose hydrolysis [70,71]. Considering the importance of the interaction between the CBD and the cellulose fiber, we performed a docking analysis and verified that the phosphorylated form of Cel7A presents greater affinity for the cellulolytic fiber than the non-phosphorylated version, bearing in mind that the binding energy value increases with the size of the carbohydrate chain. Moreover, phosphorylated Cel7A forms more hydrogen bonds with the cellulose fiber than Cel7A in its natural state. Thus, we suggest that the number of hydrogen interactions formed under the influence of a nearby phosphate group may promote the stabilization of the enzyme onto cellulose, thereby interfering with CD complexation, and influencing cellulose hydrolysis. We also speculate that phosphorylation is a way to control biomass degradation, since the increased hydrogen bonds might somewhat induce the immobilization of the protein. Since cellulases need to pass through the cellulose surface to break it, an immobilized enzyme might indicate a lack of productivity [72,73]. However, the opposite may also be inferred, since the dissociation time of Cel7A is much longer than the formation of cellobiose product itself, giving the enzyme a higher chance of feeding its active tunnel with the substrate [74]. Finally, phosphorylation can also exert an inhibitory effect on Cel7A, since the removal of phosphates by some phosphatases may mediate cellulase activation [75].

Two other glycosyl hydrolases were also identified: a GH3 β-xylosidase and a GH115. In particular, β-xylosidase (BXL1) catalyzes the cleavage of xylobiose and operates on the non-reducing ends of short xylo-oligosaccharides to free xylose [76,77]. Its function is very important in the degradation of xylan due to removal of the end product, which inhibits the action of endoxylanases during xylan hydrolysis [78]. Interestingly, β-xylosidases from filamentous fungi are associated with the mycelium in the initial stages of growth, and may remain associated with the cell during the entire growth period or be subsequently released into the environment by secretion or as a result of cell lysis [79–81]. Phosphorylation of β-xylosidases has not been previously described, while our results suggest that post-translational modifications regulate its activity. However, they seem to do so in an opposite way compared to Cel7A. In fact, dephosphorylation of β-xylosidase increased its activity. The role of the phosphorylation of this enzyme should be the subject of another study, that, together with the present results, would allow a deeper understanding of why these glycosyl hydrolases are phosphorylated in *T. reesei*.

In our phosphoproteome we identified some Heat Shock Proteins (HSPs), Hsp70 and Hsp104, which act as molecular chaperons and are mainly involved in the regulation of fungal morphogenesis, being important for the initial folding of polypeptide aggregates and thus protein stabilization [82]. Moreover, Hsp70 is also involved in the modulation of the activity of signal transducers such as protein kinase A, protein kinase C, and protein phosphatase [83], under normal growth conditions or stress. On the other hand, Hsp30 is a single integral plasma membrane HSP that limits excessive ATP consumption by the plasma membrane H^+-ATPase during prolonged exposure to stress or glucose limitation [84].

Concerning fungal metabolism, we identified a widely characterized metalloenzyme from the metabolic pathway of glycolysis expressed during biomass degradation, enolase (2-phospho-D-glycerate hydrolyase). This enzyme catalyzes the dehydration of 2-phospho-D-glycerate to phosphoenolpyruvate. Several studies have shown that enolase is a multifaceted protein with multiple roles at diverse subcellular localizations, such as on the cell wall, cell membranes, and nucleus [84], and is secreted during hyphal growth of various fungi [85]. For example, enolase is involved in laminin binding in *Staphylococcus aureus* [86] and in inhibition of adhesion of *P. brasiliensis* to epithelial cell cultures [87], owing to its ability to bind to both fibronectin and plasminogen [87,88].

Another very important protein involved in glycolysis, transaldolase, was identified in this study. This protein is an enzyme involved in the non-oxidative phase of the pentose phosphate pathway (PPP). In particular, this enzyme catalyzes a reaction where a three-carbon fragment is removed from sedoheptulose-7-phosphate and condensed with glyceraldehyde 3-phosphate to form fructose 6-phosphate and erythrose-4-phosphate tetrose, and, together with transketolase, links the PPP to glycolysis [89]. Transaldolases have been identified in a wide range of microorganisms, including several fungal species, such as *Moniliella megachiliensis*, that specifically express them under oxidative and osmotic stress [90].

Conclusion

Sugarcane bagasse is a complex carbon source for the fungus to sense and respond to. Once *T. reesei* starts growing on this nutrient, it activates different signaling pathways that regulate all cellular aspects. It is known that regulation of holocellulase expression occurs through the activation of transcription factors that act as inducers or repressors. However, the results found in this work suggested that also post-translational regulation plays a role in determining cellulase activity. This work approached the broad phosphorylation pattern that is produced when *T. reesei* is cultivated on sugarcane bagasse and provided novel information about several proteins and phosphosites that had not been previously described. Altogether, these findings provided useful knowledge for a deeper understanding of the regulation of protein activity and signaling pathways involved in biomass degradation.

Author contributions

Roberto N Silva: Conceptualization, Methodology, Writing – Original Draft. Antônio Rossi Filho: Conceptualization, Methodology. Maíra Pompeu Martins: Conceptualization, Methodology. Wellington Ramos Pedersoli: Conceptualization, Methodology, Investigation, Formal analysis, Validation, Writing – Original Draft. Liliane Fraga Costa Ribeiro: Investigation, Formal analysis, Validation, Writing – Original Draft. Amanda Cristina Campos Antoniêto: Investigation, Formal analysis, Validation (*T. reesei* manipulation and enzymatic assays). Renato Graciano de Paula: Writing – Original Draft. Cláudia Batista Carraro, Iasmin Cartaxo Taveira, David Batista Maués and Rafael Silva-Rocha: Formal analysis (bioinformatic analyses). André Ricardo de Lima Damasio: Investigation (protein purification from *Aspergillus nidulans*). All authors: Writing – Review & Editing.

Declaration of Competing Interest

All authors declare no financial and personal relationships with other people or organizations that could inappropriately influence the work.

Acknowledgments

This work was supported by Fundação de Amparo à Pesquisa do Estado de São Paulo (FAPESP, grant number 2016/20358-5 and 19/11655-4), and Coordenação de Aperfeiçoamento de Pessoal de Nível Superior (CAPES). RNS is also support by National Council for Scientific and Technological Development (CNPq) (grant number 301921/2018-0). We are also thankful to Professor Vitor Marcel Faça from the Cancer Proteomics Laboratory of the Medical School of Ribeirao Preto (FMRP-USP) for helping with the gel-based UPLC-MS/MS experiments, and the Mass Spectrometry facility of the Brazilian Biosciences National Laboratory (LNBio), CNPEM, Campinas, São Paulo, Brazil, for the support on the phosphoproteomic identification in gel-free samples. We also acknowledge the technical assistance of Bianca Alves Pauletti e Romênia Ramos Domingues from the Mass Spectrometry facility of the LNBio. .

Supplementary materials

Supplementary material associated with this article can be found, in the online version, at doi:10.1016/j.btre.2021.e00652.

References

[1] L. Kredics, L. Hatvani, S. Naeimi, P. Körmöczi, L. Manczinger, C. Vágvölgyi, I. Druzhinina, Biodiversity of the Genus Hypocrea/Trichoderma in Different Habitats, in: V. Gupta, M. Schmoll, A. Herrera-Estrella, R. Upadhyay, I. Druzhinina, M. Tuohy (Eds.),, Biotechnol. Biol. Trichoderma, Elsevier (2014).

[2] C.P. Kubicek, M. Komon-Zelazowska, I.S. Druzhinina, Fungal genus Hypocrea/Trichoderma: from barcodes to biodiversity, J. Zhejiang Univ. Sci. B. 9 (2008) 753–763, https://doi.org/10.1631/jzus.B0860015.

[3] F.A.C. Lopes, A.S. Steindorff, A.M. Geraldine, R.S. Brandão, V.N. Monteiro, M. Lobo, A.S.G. Coelho, C.J. Ulhoa, R.N. Silva, Biochemical and metabolic profiles of Trichoderma strains isolated from common bean crops in the Brazilian Cerrado, and potential antagonism against Sclerotinia sclerotiorum, Fungal Biol. 116 (2012) 815–824, https://doi.org/10.1016/j.funbio.2012.04.015.

[4] L. Hoyos-Carvajal, S. Orduz, J. Bissett, Genetic and metabolic biodiversity of Trichoderma from Colombia and adjacent neotropic regions, Fungal Genet. Biol. (2009), https://doi.org/10.1016/j.fgb.2009.04.006.

[5] C.P. Kubicek, Systems biological approaches towards understanding cellulase production by Trichoderma reesei, J. Biotechnol. 163 (2013) 133–142, https://doi.org/10.1016/j.jbiotec.2012.05.020.

[6] D. Martinez, R.M. Berka, B. Henrissat, M. Saloheimo, M. Arvas, S.E. Baker, J. Chapman, O. Chertkov, P.M. Coutinho, D. Cullen, E.G.J. Danchin, I.V. Grigoriev, P. Harris, M. Jackson, C.P. Kubicek, C.S. Han, I. Ho, L.F. Larrondo, A.L. De Leon, J. K. Magnuson, S. Merino, M. Misra, B. Nelson, N. Putnam, B. Robbertse, A. A. Salamov, M. Schmoll, A. Terry, N. Thayer, A. Westerholm-Parvinen, C.L. Schoch, J. Yao, R. Barbote, M.A. Nelson, C. Detter, D. Bruce, C.R. Kuske, G. Xie, P. Richardson, D.S. Rokhsar, S.M. Lucas, E.M. Rubin, N. Dunn-Coleman, M. Ward, T.S. Brettin, Genome sequencing and analysis of the biomass-degrading fungus Trichoderma reesei (syn. Hypocrea jecorina), Nat. Biotechnol. (2008), https://doi.org/10.1038/nbt1403.

[7] L.Dos Santos Castro, W.R. Pedersoli, A.C.C. Antoni?to, A.S. Steindorff, R. Silva-Rocha, N.M. Martinez-Rossi, A. Rossi, N.A. Brown, G.H. Goldman, V.M. Fa?a, G. F. Persinoti, R.N. Silva, Comparative metabolism of cellulose, sophorose and glucose in Trichoderma reesei using high-throughput genomic and proteomic analyses, Biotechnol. Biofuels. 7 (2014), https://doi.org/10.1186/1754-6834-7-41.

[8] A. Cziferszky, R.L. Mach, C.P. Kubicek, Phosphorylation positively regulates DNA binding of the carbon catabolite repressor Cre1 of Hypocrea jecorina (Trichoderma reesei), J. Biol. Chem. 277 (2002) 14688–14694, https://doi.org/10.1074/jbc.M200744200.

[9] L. Han, Y. Tan, W. Ma, K. Niu, S. Hou, W. Guo, Y. Liu, X. Fang, Precision Engineering of the Transcription Factor Cre1 in Hypocrea jecorina (Trichoderma reesei) for Efficient Cellulase Production in the Presence of Glucose, Front. Bioeng. Biotechnol. 8 (2020), https://doi.org/10.3389/fbioe.2020.00852.

[10] T. Yamamoto, K. Nakayama, H. Hirano, T. Tomonaga, Y. Ishihama, T. Yamada, T. Kondo, Y. Kodera, Y. Sato, N. Araki, H. Mamitsuka, N. Goshima, Integrated view of the human chromosome x-centric proteome project, J. Proteome Res. 12 (2013) 58–61, https://doi.org/10.1021/pr300844p.

[11] S. Morandell, T. Stasyk, K. Grosstessner-Hain, E. Roitinger, K. Mechtler, G.K. Bonn, L.A. Huber, Phosphoproteomics strategies for the functional analysis of signal transduction, Proteomics 6 (2006) 4047–4056, https://doi.org/10.1002/pmic.200600058.

[12] E.V. Nguyen, S.Y. Imanishi, P. Haapaniemi, A. Yadav, M. Saloheimo, G.L. Corthals, T.M. Pakula, Quantitative Site-Specific Phosphoproteomics of Trichoderma reesei Signaling Pathways upon Induction of Hydrolytic Enzyme Production, J. Proteome Res. 15 (2016) 457–467, https://doi.org/10.1021/acs.jproteome.5b00796.

[13] L. Jain, D. Agrawal, Performance evaluation of fungal cellulases with dilute acid pretreated sugarcane bagasse: A robust bioprospecting strategy for biofuel enzymes, Renew. Energy. 115 (2018) 978–988, https://doi.org/10.1016/j.renene.2017.09.021.

[14] C.L. Joppert, M.M. dos Santos, H.K.M. Costa, E.M. dos Santos, J.R. Moreira Simões, Energetic shift of sugarcane bagasse using biogas produced from sugarcane vinasse in Brazilian ethanol plants, Biomass Bioenergy 107 (2017) 63–73, https://doi.org/10.1016/j.biombioe.2017.09.011.

[15] M. Rastogi, S. Shrivastava, Recent advances in second generation bioethanol production: An insight to pretreatment, saccharification and fermentation processes, Renew. Sustain. Energy Rev. (2017), https://doi.org/10.1016/j.rser.2017.05.225.

[16] A. Amore, S. Giacobbe, V. Faraco, Regulation of cellulase and hemicellulase gene expression in fungi, Curr Genom. 14 (2013) 230–249, https://doi.org/10.2174/1389202911314040002.

[17] I.S. Druzhinina, C.P. Kubicek, Genetic engineering of Trichoderma reesei cellulases and their production, John Wiley and Sons Inc., Hoboken, 2017, https://doi.org/10.1111/1751-7915.12726.

[18] M. Schmoll, A. Schuster, N. Silva Rdo, C.P. Kubicek, The G-alpha protein GNA3 of Hypocrea jecorina (Anamorph Trichoderma reesei) regulates cellulase gene expression in the presence of light, Eukaryot. Cell 8 (2009) 410–420, https://doi.org/10.1128/EC.00256-08.

[19] L.dos Santos Castro, R.G. de Paula, A.C.C. Antoniêto, G.F. Persinoti, R. Silva-Rocha, R.N. Silva, Understanding the Role of the Master Regulator XYR1 in Trichoderma reesei by Global Transcriptional Analysis, Front. Microbiol. 7 (2016) 175, https://doi.org/10.3389/fmicb.2016.00175.

[20] R.G. de Paula, A.C.C. Antoniêto, C.B. Carraro, D.C.B. Lopes, G.F. Persinoti, N.T. A. Peres, N.M. Martinez-Rossi, R. Silva-Rocha, R.N. Silva, The Duality of the MAPK Signaling Pathway in the Control of Metabolic Processes and Cellulase Production in Trichoderma reesei, Sci. Rep. 8 (2018) 14931, https://doi.org/10.1038/s41598-018-33383-1.

[21] A.C.C. Antoniêto, R.G. de Paula, L. dos S. Castro, R. Silva-Rocha, G.F. Persinoti, R. N. Silva, Trichoderma reesei CRE1-mediated Carbon Catabolite Repression in Response to Sophorose Through RNA Sequencing Analysis, Curr. Genom. 17 (2016) 119–131, https://doi.org/10.2174/1389202917666151116212901.

[22] W.R. de Souza, P.F. de Gouvea, M. Savoldi, I. Malavazi, L.A. de Souza Bernardes, M.H.S. Goldman, R.P. de Vries, J.V de Castro Oliveira, G.H. Goldman, Transcriptome analysis of Aspergillus niger grown on sugarcane bagasse, Biotechnol. Biofuels 4 (2011) 40, https://doi.org/10.1186/1754-6834-4-40.

[23] G. Miller, Use of dinitrosalicylic acid reagent for determination of reducing sugar, Anal Chem 31 (1959) 426–428, https://doi.org/10.1021/ac60147a030.

[24] V.N. Monteiro, R. do Nascimento Silva, A.S. Steindorff, F.T. Costa, E.F. Noronha, C. A. Ricart, M.V de Sousa, M.H. Vainstein, C.J. Ulhoa, New insights in Trichoderma harzianum antagonism of fungal plant pathogens by secreted protein analysis, Curr. Microbiol. 61 (2010) 298–305, https://doi.org/10.1007/s00284-010-9611-8.

[25] U.K. Laemmli, Cleavage of structural proteins during the assembly of the head of bacteriophage T4, Nature 227 (1970) 680–685.

[26] H. Horn, E.M. Schoof, J. Kim, X. Robin, M.L. Miller, F. Diella, A. Palma, G. Cesareni, L.J. Jensen, R. Linding, KinomeXplorer: An integrated platform for kinome biology studies, Nat. Methods (2014), https://doi.org/10.1038/nmeth.2968.

[27] A. Hideno, H. Inoue, K. Tsukahara, S. Yano, X. Fang, T. Endo, S. Sawayama, Production and characterization of cellulases and hemicellulases by Acremonium cellulolyticus using rice straw subjected to various pretreatments as the carbon source, Enzyme Microb. Technol. 48 (2011) 162–168, https://doi.org/10.1016/j.enzmictec.2010.10.005.

[28] A.C.C. Antoniêto, W. Ramos Pedersoli, L. dos Santos Castro, R. da Silva Santos, A. H. da S. Cruz, K.M.V. Nogueira, R. Silva-Rocha, A. Rossi, R.N. Silva, Deletion of pH Regulator pac-3 Affects Cellulase and Xylanase Activity during Sugarcane Bagasse Degradation by Neurospora crassa, PLoS One 12 (2017), e0169796, https://doi.org/10.1371/journal.pone.0169796.

[29] Z. Xiao, R. Storms, A. Tsang, Microplate-based carboxymethylcellulose assay for endoglucanase activity, Anal. Biochem. 342 (2005) 176–178, https://doi.org/10.1016/j.ab.2005.01.052.

[30] L.D.S. Castro, A.C.C. Antoniêto, W.R. Pedersoli, R. Silva-Rocha, G.F. Persinoti, R. N. Silva, Expression pattern of cellulolytic and xylanolytic genes regulated by transcriptional factors XYR1 and CRE1 are affected by carbon source in Trichoderma reesei, Gene Expr. Patterns. 14 (2014) 88–95, https://doi.org/10.1016/j.gep.2014.01.003.

[31] J. Yang, Y. Zhang, I-TASSER server: new development for protein structure and function predictions, Nucleic Acids Res.. 43 (2015) W174–W181. https://doi.org/10.1093/nar/gkv342.

[32] J. Yang, R. Yan, A. Roy, D. Xu, J. Poisson, Y. Zhang, The I-TASSER suite: Protein structure and function prediction, Nat. Methods 12 (2014) 7–8, https://doi.org/10.1038/nmeth.3213.

[33] G.M. Morris, R. Huey, W. Lindstrom, M.F. Sanner, R.K. Belew, D.S. Goodsell, A. J. Olson, AutoDock4 and AutoDockTools4: Automated docking with selective receptor flexibility, J. Comput. Chem. 30 (2009) 2785–2791, https://doi.org/10.1002/jcc.21256.

[34] S.M.D. Rizvi, S. Shakil, M. Haneef, A simple click by click protocol to perform docking: AutoDock 4.2 made easy for non-bioinformaticians, EXCLI J. 12 (2013) 831–857.

[35] D.S. HUEY, R. MORRIS, G.M. OLSON, A.J. GOODSELL, Software News and Update A Semiempirical Free Energy Force Field with Charge-Based Desolvation, J. Comput. Chem. 28 (2007) 1145–1152, https://doi.org/10.1002/jcc.

[36] X. Dou, D. Wu, W. An, J. Davies, S.B. Hashmi, L. Ukil, S.A. Osmani, The PHOA and PHOB cyclin-dependent kinases perform an essential function in Aspergillus nidulans, Genetics 165 (2003) 1105–1115.

[37] M. Wang, M. Zhang, L. Li, Y. Dong, Y. Jiang, K. Liu, R. Zhang, B. Jiang, K. Niu, X. Fang, Role of Trichoderma reesei mitogen-activated protein kinases (MAPKs) in cellulase formation, Biotechnol. Biofuels 10 (2017) 99, https://doi.org/10.1186/s13068-017-0789-x.

[38] X. Pan, J. Heitman, Protein kinase A operates a molecular switch that governs yeast pseudohyphal differentiation, Mol. Cell. Biol. 22 (2002) 3981–3993, https://doi.org/10.1128/mcb.22.12.3981-3993.2002.

[39] C.P. De Souza, S.B. Hashmi, A.H. Osmani, P. Andrews, C.S. Ringelberg, J. C. Dunlap, S.A. Osmani, Functional Analysis of the Aspergillus nidulans Kinome, PLoS One 8 (2013) e58008.

[40] C. Johnson, H.K. Kweon, D. Sheidy, C.A. Shively, D. Mellacheruvu, A. I. Nesvizhskii, P.C. Andrews, A. Kumar, The yeast Sks1p kinase signaling network regulates pseudohyphal growth and glucose response, PLoS Genet. 10 (2014), e1004183, https://doi.org/10.1371/journal.pgen.1004183.

[41] C. Divne, J. Ståhlberg, T.T. Teeri, T.A. Jones, High-resolution crystal structures reveal how a cellulose chain is bound in the 50 Å long tunnel of cellobiohydrolase I from Trichoderma reesei, J. Mol. Biol. 275 (1998) 309–325, https://doi.org/10.1006/jmbi.1997.1437.

[42] R.L. Silveira, M. Skaf, Concerted motions and large-scale structural fluctuations of Trichoderma reesei Cel7A cellobiohydrolase, Phys. Chem. Chem. Phys. 20 (2018) 7498–7507, https://doi.org/10.1039/C8CP00101D.

[43] E. Kanshin, L.-P. Bergeron-Sandoval, S.S. Isik, P. Thibault, S.W. Michnick, A cell-signaling network temporally resolves specific versus promiscuous phosphorylation, Cell Rep 10 (2015) 1202–1214, https://doi.org/10.1016/j.celrep.2015.01.052.

[44] Y. Liu, M.R. Chance, Integrating phosphoproteomics in systems biology, Comput. Struct. Biotechnol. J. 10 (2014) 90–97, https://doi.org/10.1016/j.csbj.2014.07.003.

[45] P. Ghorai, M. Irfan, A. Narula, A. Datta, A comprehensive analysis of Candida albicans phosphoproteome reveals dynamic changes in phosphoprotein abundance during hyphal morphogenesis, Appl. Microbiol. Biotechnol. 102 (2018) 9731–9743, https://doi.org/10.1007/s00253-018-9303-z.

[46] S.D. Willger, Z. Liu, R.A. Olarte, M.E. Adamo, J.E. Stajich, L.C. Myers, A. N. Kettenbach, D.A. Hogan, Analysis of the Candida albicans phosphoproteome, Eukaryot. Cell. 14 (2015) 474–485, https://doi.org/10.1128/EC.00011-15.

[47] J.A. Ubersax, J.E. Ferrell, Mechanisms of specificity in protein phosphorylation, Nat. Rev. Mol. Cell Biol. 8 (2007) 530–541, https://doi.org/10.1038/nrm2203.

[48] A.A. Kulkarni, A.T. Abul-Hamd, R. Rai, H. El Berry, T.G. Cooper, Gln3p Nuclear Localization and Interaction with Ure2p in Saccharomyces cerevisiae, J. Biol. Chem. 276 (2001) 32136–32144, https://doi.org/10.1074/jbc.M104580200.

[49] G.P. Borin, C.C. Sanchez, E.S. de Santana, G.K. Zanini, R.A.C. dos Santos, A. de Oliveira Pontes, A.T. de Souza, R.M.M.T.S. Dal'Mas, D.M. Riaño-Pachón, G. H. Goldman, J.V. de C. Oliveira, Comparative transcriptome analysis reveals different strategies for degradation of steam-exploded sugarcane bagasse by Aspergillus niger and Trichoderma reesei, BMC Genom. 18 (2017), https://doi.org/10.1186/s12864-017-3857-5.

[50] G. Borin, C. Sanchez, A. De Souza, E. De Santana, A. De Souza, A. Leme, F. Squina, M. Buckeridge, G. Goldman, J. De Castro Oliveira, Comparative secretome analysis of Trichoderma reesei and Aspergillus niger during growth on sugarcane biomass, PLoS One 10 (2015) 1–20, https://doi.org/10.1371/journal.pone.0129275.

[51] A.C.C. Antonieto, K.M.V. Nogueira, R.G. de Paula, L.C. Nora, M.H.A. Cassiano, M.-E. Guazzaroni, F. Almeida, T.A. da Silva, L.N.A. Ries, L.J. de Assis, G.H. Goldman, R.N. Silva, R. Silva-Rocha, A Novel Cys2His2 Zinc Finger Homolog of AZF1 Modulates Holocellulase Expression in Trichoderma reesei, MSystems (2019) 4, https://doi.org/10.1128/msystems.00161-19.

[52] L. Martins-Santana, R.G. de Paula, A. Gomes Silva, D. Christian Borges Lopes, R. do Nascimento Silva, R. Silva-Rocha, CRZ1 regulator and calcium cooperatively modulate holocellulases gene expression in Trichoderma reesei QM6a, 2020, https://doi.org/10.1590/1678-4685-GMB-2019-0244.

[53] M. Wang, Q. Zhao, J. Yang, B. Jiang, F. Wang, K. Liu, X. Fang, A mitogen-activated protein kinase Tmk3 participates in high osmolarity resistance, cell wall integrity maintenance and cellulase production regulation in Trichoderma reesei, PLoS One 8 (2013) e72189, https://doi.org/10.1371/journal.pone.0072189.

[54] F. Chen, X.-Z. Chen, X.-Y. Su, L.-N. Qin, Z.-B. Huang, Y. Tao, Z.-Y. Dong, An Ime2-like mitogen-activated protein kinase is involved in cellulase expression in the filamentous fungus Trichoderma reesei, Biotechnol. Lett. 37 (2015) 2055–2062, https://doi.org/10.1007/s10529-015-1888-z.

[55] M.D. Mendenhall, A.E. Hodge, Regulation of Cdc28 Cyclin-Dependent Protein Kinase Activity during the Cell Cycle of the Yeast Saccharomyces cerevisiae, Microbiol, Mol. Biol. Rev. (1998), https://doi.org/10.1128/mmbr.62.4.1191-1243.1998.

[56] K.T. Lee, Y.S. So, D.H. Yang, K.W. Jung, J. Choi, D.G. Lee, H. Kwon, J. Jang, L. L. Wang, S. Cha, G.L. Meyers, E. Jeong, J.H. Jin, Y. Lee, J. Hong, S. Bang, J.H. Ji, G. Park, H.J. Byun, S.W. Park, Y.M. Park, G. Adedoyin, T. Kim, A.F. Averette, J. S. Choi, J. Heitman, E. Cheong, Y.H. Lee, Y.S. Bahn, Systematic functional analysis of kinases in the fungal pathogen Cryptococcus neoformans, Nat. Commun. (2016), https://doi.org/10.1038/ncomms12766.

[57] H. Liu, S. Zhang, J. Ma, Y. Dai, C. Li, X. Lyu, C. Wang, J.R. Xu, Two Cdc2 Kinase Genes with Distinct Functions in Vegetative and Infectious Hyphae in Fusarium graminearum, PLoS Pathog (2015), https://doi.org/10.1371/journal.ppat.1004913.

[58] S. Ren, M. Yang, Y. Li, F. Zhang, Z. Chen, J. Zhang, G. Yang, Y. Yue, S. Li, F. Ge, S. Wang, Global phosphoproteomic analysis reveals the involvement of phosphorylation in aflatoxins biosynthesis in the pathogenic fungus aspergillus flavus, Sci. Rep. 6 (2016) 1–14, https://doi.org/10.1038/srep34078.

[59] E.K. Shwab, P.R. Juvvadi, G. Waitt, E.J. Soderblom, M.A. Moseley, N.I. Nicely, W. J. Steinbach, Phosphorylation of Aspergillus fumigatus PkaR impacts growth and cell wall integrity through novel mechanisms, FEBS Lett. 591 (2017) 3730–3744, https://doi.org/10.1002/1873-3468.12886.

[60] A. Lafon, J.-A. Seo, K.-H. Han, J.-H. Yu, C. d'Enfert, The heterotrimeric G-protein GanB(alpha)-SfaD(beta)-GpgA(gamma) is a carbon source sensor involved in early cAMP-dependent germination in Aspergillus nidulans, Genetics 171 (2005) 71–80, https://doi.org/10.1534/genetics.105.040584.

[61] C. Ziv, R. Gorovits, O. Yarden, Carbon source affects PKA-dependent polarity of Neurospora crassa in a CRE-1-dependent and independent manner, Fungal Genet. Biol. 45 (2008) 103–116, https://doi.org/10.1016/j.fgb.2007.05.005.

[62] A. Schuster, D. Tisch, V. Seidl-Seiboth, C.P. Kubicek, M. Schmoll, Roles of protein kinase A and adenylate cyclase in light-modulated cellulase regulation in Trichoderma reesei, Appl Env. Microbiol. 78 (2012) 2168–2178, https://doi.org/10.1128/AEM.06959-11.

[63] D. Esser, T.K. Pham, J. Reimann, S.V. Albers, B. Siebers, P.C. Wright, Change of carbon source causes dramatic effects in the phospho-proteome of the archaeon Sulfolobus solfataricus, J. Proteome Res. 11 (2012) 4823–4833, https://doi.org/10.1021/pr300190k.

[64] R.G. de Paula, A.C.C. Antoniêto, L.F.C. Ribeiro, C.B. Carraro, K.M.V. Nogueira, D.C. B. Lopes, A.C. Silva, M.T. Zerbini, W.R. Pedersoli, M. do N. Costa, R.N. Silva, New Genomic Approaches to Enhance Biomass Degradation by the Industrial Fungus *Trichoderma reesei*, Int. J. Genomics. 2018 (2018) 1–17.

[65] N.S. Sweilem, M.L. Sinnott, The hydrolysis of cellulose by Trichoderma reesei CBHI and -II in relation to the coupled vectorial process hypothesis, Biochemistry 35 (1996) undefined-undefined.

[66] A. Borisova, E. Eneyskaya, K. Bobrov, S. Jana, A. Logachev, D. Polev, A. Lapidus, F. Ibatullin, U. Saleem, M. Sandgren, C. Payne, A. Kulminskaya, J. Stahlberg, Sequencing, biochemical characterization, crystal structure and molecular dynamics of cellobiohydrolase Cel7A from Geotrichum candidum 3C, FEBS J 282 (2015) 4515–4537, https://doi.org/10.1111/febs.13509.

[67] H. Nishi, K. Hashimoto, A.R. Panchenko, Phosphorylation in Protein-Protein Binding: Effect on Stability and Function, Structure. 19 (2011) 1807–1815. https://doi.org/https://doi.org/10.1016/j.str.2011.09.021.

[68] J.-K. Yang, W. Xiong, F.-Y. Chen, L. Xu, Z.-G. Han, Aromatic amino acids in the cellulose binding domain of Penicillium crustosum endoglucanase EGL1 differentially contribute to the cellulose affinity of the enzyme, PLoS One 12 (2017), e0176444.

[69] T. Yui, H. Shiiba, Y. Tsutsumi, S. Hayashi, T. Miyata, F. Hirata, Systematic docking study of the carbohydrate binding module protein of Cel7A with the cellulose Ialpha crystal model, J Phys Chem B 114 (2010) 49–58, https://doi.org/10.1021/jp908249r.

[70] T. Jeoh, M.J. Cardona, N. Karuna, A.R. Mudinoor, J. Nill, Mechanistic kinetic models of enzymatic cellulose hydrolysis—A review, Biotechnol. Bioeng. 114 (2017) 1369–1385, https://doi.org/10.1002/bit.26277.

[71] A. Griffo, B.J.M. Rooijakkers, H. Hähl, K. Jacobs, M.B. Linder, P. Laaksonen, Binding Forces of Cellulose Binding Modules on Cellulosic Nanomaterials, Biomacromolecules 20 (2019) 769–777, https://doi.org/10.1021/acs.biomac.8b01346.

[72] J.D. Nill, T. Jeoh, The Role of Evolving Interfacial Substrate Properties on Heterogeneous Cellulose Hydrolysis Kinetics, ACS Sustain. Chem. Eng. 8 (2020) 6722–6733, https://doi.org/10.1021/acssuschemeng.0c00779.

[73] A.R. Mudinoor, P.M. Goodwin, R.U. Rao, N. Karuna, A. Hitomi, J. Nill, T. Jeoh, Interfacial molecular interactions of cellobiohydrolase Cel7A and its variants on cellulose, Biotechnol. Biofuels. 13 (2020) 10, https://doi.org/10.1186/s13068-020-1649-7.

[74] R. Kont, J. Kari, K. Borch, P. Westh, P. Väljamäe, Inter-domain Synergism Is Required for Efficient Feeding of Cellulose Chain into Active Site of Cellobiohydrolase Cel7A, J. Biol. Chem. 291 (2016) 26013–26023, https://doi.org/10.1074/jbc.M116.756007.

[75] A. Rodriguez-Iglesias, M. Schmoll, Protein phosphatases regulate growth, development, cellulases and secondary metabolism in Trichoderma reesei, Sci. Rep. 9 (2019) 10995, https://doi.org/10.1038/s41598-019-47421-z.

[76] L.E. Rasmussen, H.R. Sørensen, J. Vind, A. Viksø-Nielsen, Mode of action and properties of the β-xylosidases from Talaromyces emersonii and Trichoderma reesei, Biotechnol. Bioeng. 94 (2006) 869–876, https://doi.org/10.1002/bit.20908.

[77] H.R. Sorensen, A.S. Meyer, S. Pedersen, Enzymatic hydrolysis of water-soluble wheat arabinoxylan. 1. Synergy between α- <scp>L</scp>-arabinofuranosidases, endo-1,4-β-xylanases, and β-xylosidase activities, Biotechnol. Bioeng. 81 (2003) 726–731, https://doi.org/10.1002/bit.10519.

[78] A. Sunna, G. Antranikian, Xylanolytic enzymes from fungi and bacteria, Crit. Rev. Biotechnol. 17 (1997) 39–67, https://doi.org/10.3109/07388559709146606.

[79] K.K.Y. Wong, J.N. Saddler, Trichoderma Xylanases, Their Properties and Application, Crit. Rev. Biotechnol. 12 (1992) 413–435, https://doi.org/10.3109/07388559209114234.

[80] T. Iembo, M.O. Azevedo, C.B.Jr., E.X.F. Filho, Purification and partial characterization of a new β-xylosidase from Humicola grisea var. thermoidea,

World J. Microbiol. Biotechnol. 22 (2006) 475–479, https://doi.org/10.1007/s11274-005-9059-3.
[81] T. Ito, E. Yokoyama, H. Sato, M. Ujita, T. Funaguma, K. Furukawa, A. Hara, Xylosidases associated with the cell surface of Penicillium herquei IFO 4674, J. Biosci. Bioeng. 96 (2003) 354–359, https://doi.org/10.1016/S1389-1723(03)90136-8.
[82] S. Tiwari, R. Thakur, J. Shankar, Role of Heat-Shock Proteins in Cellular Function and in the Biology of Fungi, 2015, https://doi.org/10.1155/2015/132635.
[83] A.C. Newton, Regulation of the ABC kinases by phosphorylation: Protein kinase C as a paradigm, Biochem. J. 370 (2003) 361–371, https://doi.org/10.1042/BJ20021626.
[84] I. Pal-Bhowmick, H.K. Vora, G.K. Jarori, Sub-cellular localization and post-translational modifications of the Plasmodium yoelii enolase suggest moonlighting functions, Malar. J. 6 (2007) 45, https://doi.org/10.1186/1475-2875-6-45.
[85] M. Breitenbach, B. Simon, G. Probst, H. Oberkofler, F. Ferreira, P. Briza, G. Achatz, A. Unger, C. Ebner, D. Kraft, R. Hirschwehr, Enolases are highly conserved fungal allergens, Int. Arch. Allergy Immunol. 113 (1997) 114–117, https://doi.org/10.1159/000237521.
[86] C.R.W. Carneiro, E. Postol, R. Nomizo, L.F.L. Reis, R.R. Brentani, Identification of enolase as a laminin-binding protein on the surface of Staphylococcus aureus, 2004, https://doi.org/10.1016/j.micinf.2004.02.003.
[87] F.C. Donofrio, A.C.A. Calil, E.T. Miranda, A.M.F. Almeida, G. Benard, C.P. Soares, S.N. Veloso, C.M. De Almeida Soares, M.J.S. Mendes Giannini, Enolase from Paracoccidioides brasiliensis: Isolation and identification as a fibronectin-binding protein, J. Med. Microbiol. 58 (2009) 706–713, https://doi.org/10.1099/jmm.0.003830-0.
[88] S.V. Nogueira, F.L. Fonseca, M.L. Rodrigues, V. Mundodi, E.A. Abi-Chacra, M. S. Winters, J.F. Alderete, C.M. De Almeida Soares, Paracoccidioides brasiliensis enolase is a surface protein that binds plasminogen and mediates interaction of yeast forms with host cells, Infect. Immun. 78 (2010) 4040–4050, https://doi.org/10.1128/IAI.00221-10.
[89] A.K. Samland, G.A. Sprenger, Transaldolase: From biochemistry to human disease, Int. J. Biochem. Cell Biol. 41 (2009) 1482–1494, https://doi.org/10.1016/j.biocel.2009.02.001.
[90] J.-Y. Liu, S.-D. Li, M.-H. Sun, Transaldolase gene Tal67 enhances the biocontrol activity of Clonostachys rosea 67-1 against Sclerotinia sclerotiorum, Biochem. Biophys. Res. Commun. 474 (2016) 503–508, https://doi.org/10.1016/j.bbrc.2016.04.133.